END

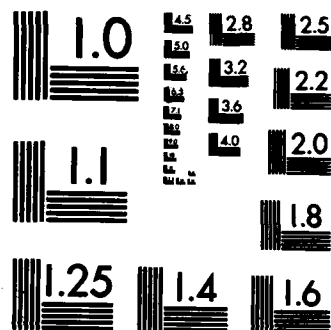MICROCOPY RESOLUTION TEST CHART
NATIONAL BUREAU OF STANDARDS-1963-A
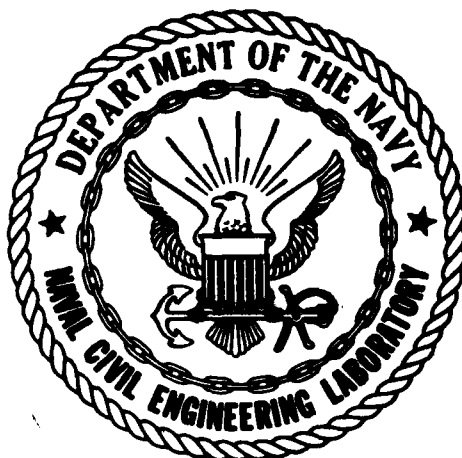
CR 85.008

NAVAL CIVIL ENGINEERING LABORATORY
Port Hueneme, California

Sponsored by
DEPARTMENT OF INTERIOR
MINERAL MANAGEMENT SERVICE
NAVAL FACILITIES ENGINEERING COMMAND

AD-A157 709

WAVE FORCE-PHASE METHOD FOR VERTICAL CYLINDERS

May 1985

An Investigation Conducted by:
Ocean Engineering Program
Civil Engineering Department
Oregon State University
Corvallis, OR 97311

DTIC FILE COPY

N62474-82-C08295

DTIC
ELECTE
JUL 1 7 1985
S   D
G

85 6 28 120

SECURITY CLASSIFICATION OF THIS PAGE (When Data Entered)

REPORT DOCUMENTATION PAGE	READ INSTRUCTIONS BEFORE COMPLETING FORM

1. REPORT NUMBER	2. GOVT ACCESSION NO.	3. RECIPIENT'S CATALOG NUMBER
CR 85.008	AD-A157709	

4. TITLE (and Subtitle)	5. TYPE OF REPORT & PERIOD COVERED
Wave Force-Phase Method for Vertical Cylinders	Final May 1984 - Feb 1985
	6. PERFORMING ORG. REPORT NUMBER

7. AUTHOR(s)	8. CONTRACT OR GRANT NUMBER(s)
John H. Nath	N62474-82-C08295

9. PERFORMING ORGANIZATION NAME AND ADDRESS	10. PROGRAM ELEMENT, PROJECT, TASK AREA & WORK UNIT NUMBERS
Ocean Engrng Prog, Civil Engrng Dept Oregon State University Corvallis, OR 97311	YF60.534.091.01 A352

11. CONTROLLING OFFICE NAME AND ADDRESS	12. REPORT DATE
Naval Civil Engineering Laboratory Port Hueneme, CA 93043	May 1985
	13. NUMBER OF PAGES 72

14. MONITORING AGENCY NAME & ADDRESS(if different from Controlling Office)	15. SECURITY CLASS. (of this report)
Dept of Interior, Mineral Mgmt Serv Tech Assessment & Research Program 647 National Ctr, Reston, VA 22091 Nav Fac Engr Cmd, Alexandria, VA 22332	Unclassified
	15a. DECLASSIFICATION DOWNGRADING SCHEDULE

16. DISTRIBUTION STATEMENT (of this Report)

Approved for public release; distribution is unlimited.

17. DISTRIBUTION STATEMENT (of the abstract entered in Block 20, if different from Report)

18. SUPPLEMENTARY NOTES

19. KEY WORDS (Continue on reverse side if necessary and identify by block number)

Wave forces, maximum force coefficient, wave phase, cylinders, Morison equation, maximum wave force prediction

20. ABSTRACT (Continue on reverse side if necessary and identify by block number)

The maximum force and its phase is determined for laboratory wave forces on smooth vertical cylinders. The maximum force coefficient, C_{pk} and the normalized phase angle, $\hat{\Phi}$ of the force with respect to the wave particle velocity, can be

DD $\begin{smallmatrix} \text{FORM} \\ 1 \text{ JAN } 73 \end{smallmatrix}$ 1473   EDITION OF 1 NOV 65 IS OBSOLETE

iii

C subscript d   C subscript m

related to the force transfer coefficients, C_d and C_m, for the Morison equation. This method enables the data to be plotted in a way that immediately shows the drag or inertia dependency for the wave/cylinder conditions. In addition, the C_d and C_m so derived are more likely to properly predict the maximum value of the force, although they may also increase the rms error between the measured force and the predicted force in the time domain.

Accession For

NTIS GRA&I
DTIC TAB
Unannounced
Justification

By
Distribution/
Availability Codes

Dist	Avail and/or Special
A|	

TABLE OF CONTENTS

INTRODUCTION

Background

The famous Morison equation (7) has been used for over 34 years to estimate wave forces on vertical cylinders when the cylinder diameter is less than approximately .05 times the wave length. Much understanding of the influence on C_d and C_m from the Reynolds number, R, the Keulegan-Carpenter number, K, the water particle orbit shape, Ω, and the relative roughness, ϵ/D, has been gained since 1950. It might seem that little additional information could be added to the bank of knowledge on this subject. However, the features of this subject are complex, involving, but not limited to, the wave theory used in the prediction, wave irregularities and nonlinearities, cylinder shape and orientation, vortex shedding, and the cylinder surface roughness. Therefore, new approaches are continually being developed that are worth consideration in order to make safer and more economical predictions of these wave forces.

This paper presents an alternative way of utilizing only the maximum force, in conjunction with the phase angle to it, to better organize laboratory data, to better display the relative influence between the water velocity and acceleration, and perhaps to better estimate C_d and C_m. Some features of this method have been published by others (1,16,17), and there may be others that are unknown to the writer. However, this may be a first presentation of how the results from certain laboratory testing can be extended to prototype scales.

The Morison equation for the force per unit of length on a vertical cylinder, F, is written as

$$F = \frac{1}{2} C_d \, D \, \rho \, u|u| + C_m \, \frac{\pi D^2}{4} \, \rho \, \dot{u} \qquad (1)$$

1

where C_d is the drag coefficient, D is the cylinder diameter, ρ is the fluid mass density, u is the horizontal component of the water particle velocity, C_m ($= 1 + C_a$) is the inertia coefficient (where C_a is the added mass coefficient), and $\dot{u}$ is the water particle temporal acceleration.

It is sometimes useful to know if ambient flow conditions, combined with cylinder size and roughness, result in a mostly drag-dependent force, where the maximum value of the first term of Eq. (1) is larger than, say, three times the maximum value of the second term. Or, it may be useful to know when the magnitude of the second term is larger than that of the first term. This knowledge is particularly useful for estimating the "conditioning" of force measurement data from which values of C_d and C_m have been determined. For example, where the magnitude of the second term is small, force transducer characteristics and data processing techniques are such that the values of C_m obtained are unreliable and may be widely scattered. The same is true for C_d if the relative magnitude of the second term is much larger than the first. A discourse on conditioning of data for good C_d and C_m values was given by Dean (2), which was based on a nondimensional number, itself dependent on values of C_d and C_m. The technique presented herein depends on the relative phases between the ambient velocity, acceleration, and force.

Vortex shedding from the cylinder, the conditioning of the data, and measurement and analysis equipment and methods can introduce considerable scatter to the results for both C_d and C_m. The work of Sarpkaya, which is summarized up to about 1980 or 1981 in reference (14), is quite remarkable because the water tunnel that was used produced smooth, repeatable planar oscillatory flow, which yielded very repeatable results, which in turn produced values of C_d and C_m with very little scatter. The results have been

2

valuable because they extend into fairly high Reynolds number (1.5×10^6) and Keulegan-Carpenter number (100), with β ($= R/K$) values up to 8370. Sarpkaya's work also approximately simulated the orbital motion of waves on a vertical cylinder by sliding the test cylinder, along its axis, into and out of the water tunnel test section, with varying amplitude, synchronized with the water motion period (15).

Wave flow on vertical cylinders has significant differences from the oscillatory flow in a water tunnel. First, the water surface fluctuates on the cylinder between the trough and the crest. There is considerable run-up on the flow side of the cylinder (be it at the crest or the trough of the wave) and depression on the lee side, as shown in Fig. 1. The run-up and depression influences the total forces on the cylinder in a way that has not yet been quantified in the open literature. In addition, the wave flow kinematics decay with depth for all but shallow water waves. Even in carefully controlled laboratory waves with long crests, this attenuation with depth creates unknown differences in the vortex shedding characteristics around vertical cylinders, which probably change with depth. For such waves, one should expect more scatter in laboratory results than with U-tube experiments.

Of course, in the ocean one should expect even more variation of conditions (wide scatter in the results of measurements) because of a greater degree of randomness of the wave heights and periods, various degrees of short-crestedness in the waves, influences from the proximity of other structural members, and varying degrees of surface roughness because of biofouling. In fact, considerably more scatter and uncertainty is displayed for the results reported on in (17) than displayed from the laboratory data reported on here. Short-crestedness may also be important because of the

3

influence of the wake encounter effect (3). However, controlled laboratory results are useful for gaining basic knowledge on the processes of fluid mechanics. In addition, experiments in large, controlled laboratory waves can provide transition conditions between the highly idealized U-tube experiments and the design conditions of concern in the field.

The experimental data herein provide Reynolds numbers up to 7×10^5 in steady flow and 3.1×10^5 in periodic waves. The Keulegan-Carpenter number ranges up to maximum values of about 27 in waves, and the maximum values of β are about 40,000. Some 1976 oscillatory cylinder data were also reexamined wherein the maximum Reynolds number was 7×10^5, the maximum Keulegan-Carpenter number was 63, and the maximum β was about 12,000. In the field, under maximum design conditions, one would expect Reynolds numbers in the range of from 10^6 to 2×10^7, with Keulegan-Carpenter numbers approximately in the range of from 80 to 240. The associated β values would range from about 12,000 to 80,000. Thus, the work reported herein, which was performed in the Wave Research Laboratory at Oregon State University (OSU), provides information on physical events that are transitional in scale and in fluid flow character between the U-tube experiments of Sarpkaya and the actual events in the ocean, some of which were reported by Heideman, et al., (3).

When reviewing the literature one must be careful to place the various studies into perspective. It is well known that C_m is a function of both R and K when $\beta < 6000$, but that it is approximately equal to 2.0 for all K, when $\beta > 6000$. On the other hand, C_d seems to vary somewhat with K even at $\beta = 8370$, the limiting value shown in (14). It is important to combine high K, R, and β values to approach prototype conditions in order to provide best values of C_d and C_m for design considerations. Even the field study reported

4

in (17) yielded maximum K values only on the order of 30. (It is difficult to estimate K from horizontal velocities in that publication, although maximum K values from vertical velocities were at about 15.) The maximum R was about 5.7×10^5, yielding maximum β values of about 19,000. The laboratory experiments in (16) had maximum K values of about 24, but R was not reported although $\beta = 200$ was alluded to, but not clearly identified as pertaining to that work. The tests in (1) covered K values up to 40 and again R values were not reported, although they must have been low because the largest cylinder diameter was 3 inches and the largest wave period was 3.5 s.

The force-phase method reported herein has promise of reducing some of the scatter in C_d and C_m by means of a suggested alternative method of data reduction and analysis. At least the major source of the scatter is identified to be the shedding of vortices and how they influence the phase between the force measurement and the ambient velocity. Some changes in the analysis were conceived by observing the relative phases in time between the water profile or velocity measurements (which are theoretically in phase), the computed acceleration, and the force measurement. (Details of these experiments will be given later.) An example where the force is nearly in phase with the accleration is shown in Fig. 2. A case where the force is more nearly in phase with the velocity is shown in Fig. 3. These figures support the idea that if K is small, the inertia force dominates (or, the force is more nearly in phase with the acceleration). If K is larger and the cylinder is rough, then the drag force should dominate (or, the force is more nearly in phase with the velocity).

The phases to the maximum force and maximum acceleration in the general vicinity of the wave crest are shown in the figures. A crest-to-crest wave

5

was chosen for analysis instead of a trough-to-trough wave because the crests are more clearly definable for the larger and longer waves. It turned out that the three phases to the maximum values, ϕ_u, ϕ_a, and ϕ_f, (velocity, acceleration, force) are closely grouped near the right-hand crest for the waves so defined. It also turned out that the local force was much more influenced by the acceleration term than originally anticipated. In fact, in order to get a record that was more heavily influenced by the velocity term for illustration, it was necessary to use a record for a sand-roughened cylinder, as shown in Fig. 3, in addition to naving K much larger than in Fig. 2. Even so, the maximum force is still considerably influenced by the wave accelerations, as shown in the figure. Figure 3 also shows that the "measured" acceleration phase is considerably different than the acceleration phase determined from stream function, $\phi_{\psi a}$, or linear wave theories, ϕ_{La}, a condition that will be discussed in more detail later.

It would thus appear to be more direct to examine the relationship of the phase of the force with respect to the ambient velocity and acceleration in determining if conditions are drag or inertia dominant. An early paper to this effect was published (13) which briefly explains the basic ideas involved. It was shown that there may be less scatter in the data when plotting the maximum force coefficient and the phase shift than when plotting C_d and C_m.

Scope

The major purpose of this paper is to make a systematic review of a force-phase method for determi ng the forces on vertical smooth cylinders from periodic waves. Data from experiments on 8.625-inch and 12.75-inch diameter smooth aluminum cylinders will be analyzed.

6

ANALYSIS

Maximum Force Coefficient, C_μ

The maximum force coefficient, C_μ, is defined as

$$C_\mu = \frac{F_\mu}{\frac{1}{2} DL\rho u_\mu^2} \tag{2}$$

where F_μ is the maximum force on a cylinder in a wave cycle, L is the length of the cylinder over which the force is considered to act, and u_μ is the maximum horizontal velocity within the cycle. (In this paper the subscript, μ, will be used to indicate maximum values.) The maximum force can be considered near the crest or near the trough of a wave. An idealized record is presented in Fig. 4 as an illustration of several aspects of this analysis.

Phase Shift of the Force, $\hat{\phi}$

The phase shift can be defined in different ways. Since the maximum force is of prime importance for engineering, the phase shift to the force "crest" in Fig. 4, ϕ_f, will receive most of the consideration here. The same holds for the phase of the acceleration crest, ϕ_a. It is convenient to define two normalized phases for the force crest as

$$\hat{\phi} = \frac{\phi_f}{90} \tag{3}$$

and

$$\tilde{\phi} = \frac{\phi_f}{\phi_a} \tag{4}$$

wherein, if $\tilde{\phi} \rightarrow 1$, the force is dominated by the inertia effects (or, it is <u>in phase</u> with the ambient acceleration). Conversely, if $\tilde{\phi} \rightarrow 0$, the force is

dominated by the drag effects (or, it is in phase with the ambient velocity field). The phases $\hat{\phi}$ and $\tilde{\phi}$ are defined separately because it is sometimes useful to obtain ϕ_f easily and directly from a plot of $\hat{\phi}$, where $0 < \hat{\phi} < 1$. In Eq. (7) ϕ_a can be from the "measured" acceleration, or the theoretical values from the linear or stream function theories. The "measured" value is rarely equal to the stream function value and it is nearly always smaller than the linear value. Usually the value from the stream function theory was used for reasons explained later.

There is at least a passing interest in the conditions at the wave trough, so the relative phase there is defined as

$$\tilde{\phi}' = \frac{\phi_f'}{\phi_a'} .$$
(5)

For a visual determination of the phases, it can be sometimes more convenient to work to the upcrossings and downcrossings, in which case the relative, normalized phase is defined as

$$\hat{\Theta} = \frac{\Theta_f - \Theta_u}{90}$$
(6)

or

$$\tilde{\Theta} = \frac{\Theta_f - \Theta_u}{\Theta_a - \Theta_u} .$$
(7)

Some results will be presented that are based on averaging the phase at the upcrossings with the phase at the downcrossings.

Another, more computer-oriented method of determining the phase is by cross-correlation analysis, which itself can be computed by different methods. First, the cross-correlation, C_{12}, between any two signals (in this case the velocity, u, and the force, F, can be computed from

$$CR_{12} (\tau) = \int_{-\infty}^{\infty} g_1 (t) \, g_2 (t + \tau) \, dt \qquad (8)$$

where g_1 is the velocity record and g_2 is the force record. We seek the phase (or time) at which CR_{12} is maximum. In practice, the approximate τ for F_μ is known á priori. Then, τ is simply increased incrementally, calculating CR for each value, until CR_μ is reached, by evidence of a reduction in CR. Experiments with other methods, such as finding the τ at which $\partial CR/\partial \tau = 0$, and spectral methods, have required more computer time and cost. The value of τ at which CR is maximum, nondimensionalized by the wave period, and multiplied by 360°, is the force phase, or

$$\phi_f = 360 \frac{\tau}{T} . \qquad (9)$$

The phase can be also determined by either of two spectral methods. The cross-correlation and certain spectral products are Fourier transform pairs. Specifically, the spectral product, $E_{12} (f)$, is defined as

$$E_{12} (f) = S_2 (f) \, S_1^* (f) \qquad (10)$$

where

$$S_n (f) = \int_{-\infty}^{\infty} g_n (t) \, e^{-j2\pi ft} \, dt, \qquad n = 1, 2 \qquad (11)$$

and * indicates the complex conjugate. Then $CR_{12} (\tau)$ and $E_{12} (f)$ are Fourier transform pairs. However, obtaining the Fourier transform of Eq. (10) (which yields CR for <u>all</u> values of τ) usually requires more computer time than a few direct computations of Eq. (8). An alternative procedure is to recognize that

$$E_{12} (f) = CO_{12} (f) - i \, Q_{12} (f) \qquad (12)$$

9

where CO is usually termed the cospectrum and Q is the quadrature spectrum, and

$$\phi_{12}(f) = \tan^{-1} \frac{Q_{12}(f)}{CO_{12}(f)} . \qquad (13)$$

Determining ϕ from Eq. (13) also requires more computational time than the direct method of Eq. (8) if the waves are nearly periodic.

Drag and Inertia Coefficients From C_μ and $\hat{\phi}$

We now assume that the horizontal velocity at the center position of the force transducer would be (in the absence of the cylinder)

$$u = u_\mu \cos\theta \qquad (14)$$

where $\theta = \omega t$ and $\omega = 2\pi/T$, with T the wave period. Equation (1) can be non-dimensionalized by dividing both sides by $D\rho u_\mu^2/2$, substituting Eq. (14), and defining the Keulegan-Carpenter number as $K = u_\mu T/D$, so that

$$\hat{F} = C_d \cos\theta|\cos\theta| - \frac{\pi^2}{K} C_m \sin\theta . \qquad (15)$$

It is sometimes useful to approximate Eq. (15) with a linear form by either expanding the $\cos\theta|\cos\theta|$ in a Fourier series and retaining only the first term, or by utilizing the Lorentz linearization principle of equivalent work. In either case the result is

$$\hat{F} = .85 C_d \cos\theta - \frac{\pi^2}{K} C_m \sin\theta . \qquad (16)$$

The approximate maximum value of $\hat{F}$, which is actually C_μ from Eq. (2), is

$$C_\mu = [(.85 C_d)^2 + (\frac{\pi^2}{K} C_m)^2]^{1/2} \qquad (17)$$

10

and the phase between the wave crest (or u_μ) and the maximum force is

$$\phi_f = \tan^{-1}\left(-\frac{\pi^2 C_m}{.85\ K\ C_d}\right) .$$ (18)

Equations (17) and (18) are almost virtually the same as Eqs. 3 and 4 (which were not derived) in Ref. (17), except for the .85 factor, which is necessary in the linearization procedure and was omitted in Ref. (17). Combining Eqs. (17) and (18) yields

$$C_m = \frac{.85\ K\ C_d}{\pi^2}\tan(-\phi_f) .$$ (19)

By substitution into Eq. (17), and with the identity, $\cos\theta = 1/(1 + \tan^2\theta)^{1/2}$, we obtain

$$C_d = 1.176\ C_\mu\ \cos\phi_f .$$ (20)

Equation (19) can now be further simplified to

$$C_m = \frac{K\ C_\mu\ \sin(-\phi_f)}{\pi^2} .$$ (21)

Equations (17), (20), and (21) are useful for making a rough estimate of the limits of drag or inertia dominance relative to Eq. (1). A more accurate and useful estimate of C_d and C_m will be derived later where a nonlinear form similar to Eq. (1) is retained.

Now consider the phase at which either the drag or inertia term dominates the maximum force coefficient, C_μ, in Eq. (17). This is only a rough approximation because there is no universally accepted value for the concept 'domination'. For illustration, it is assumed that C_μ is influenced only 4% by the inertia term. Then

11

$$C_\mu = .85 \ C_d \ [1 + (\frac{\pi^2 \ C_m}{.85 \ K \ C_d})^2]^{1/2} \tag{22}$$

$$= .85 \ C_d \ (1.04)$$

from which, in conjunction with Eq. (18),

$$\phi_f \approx - 16° \ . \tag{23}$$

Likewise, if C_μ is to be influenced only 4% by the drag term, then

$$\phi_f \approx 74° \ . \tag{24}$$

The Morison equation need not be linearized in order to obtain C_d and C_m as functions of C_μ and ϕ_f. Consider that the maximum force occurs near the leading surface of the wave crest, some time after the maximum acceleration and before the maximum velocity, as shown in Fig. 4. In that region

$$\hat{F} = C_d \ \cos^2\theta - \frac{\pi^2}{K} \ C_m \ \sin\theta \tag{25}$$

and the maximum force will occur when

$$\frac{d\hat{F}}{d\theta} = - \ 2C_d \ \cos\theta\sin\theta - \frac{\pi^2}{K} \ C_m \ \cos\theta = 0 \ . \tag{26}$$

or,

$$\frac{d\hat{F}}{d\theta} = - \cos\theta \ (2 \ C_d \ \sin\theta + \frac{\pi^2 \ C_m}{K}) = 0 \ . \tag{27}$$

Equation (27) must hold for all time, and at the force peak, $\theta = \phi_f$, so

$$\phi_f = \sin^{-1} \ (- \frac{\pi^2 \ C_m}{2 \ K \ C_d}) \ . \tag{28}$$

12

By substitution into Eq. (25), and letting $\cos^2\theta = 1 - \sin^2\theta$,

$$\hat{F}_\mu = C_\mu = C_d (1 - \sin^2\phi_f) - \frac{\pi^2}{K} C_m \sin\phi_f , \tag{29}$$

or,

$$C_\mu = C_d[1 - (-\frac{\pi^2 C_m}{2 K C_d})^2] - \frac{\pi^2 C_m}{K} (-\frac{\pi^2 C_m}{2 K C_d}) \frac{2 C_d}{2 C_d} \tag{30}$$

or,

$$C_\mu = C_d [1 - \gamma^2 + 2 \gamma^2] \tag{31}$$

or,

$$C_d = C_\mu (1 + \gamma^2)^{-1} \tag{32}$$

where

$$\gamma = \sin (- \phi_f) = \frac{\pi^2 C_m}{2 K C_d} . \tag{33}$$

From Eq. (33)

$$C_m = \frac{2 K C_d \gamma}{\pi^2} \tag{34}$$

and by substituting Eq. (32),

$$C_m = \frac{2 K C_\mu}{\pi^2} \frac{\gamma}{1 + \gamma^2} . \tag{35}$$

If $\hat{\phi}$ and C_μ are determined experimentally, then C_d and C_m can be estimated from Eqs. (32) and (35). The coefficient C_μ is relatively independent of ϕ_f. However, ϕ_f can be influenced markedly by vortex shedding and the vagaries of the ambient flow. Laboratory data show that plots of C_μ vs. K have relatively little scatter but the opposite is true for plots of ϕ_f.

13

Since both C_d and C_m are influenced by ϕ_f, experimental values of them do have scatter.

Steady Tow Drag Coefficient

It is of interest to consider wave conditions with very large K because such values can exist for prototype (full scale) conditions in design sea state conditions. At some large K, nearly steady-state flow conditions should exist. In the OSU laboratory the maximum local K that can be obtained for the 8.625-inch diameter cylinder was about 26. However, steady-state towing was accomplished with a tow carriage, up to Reynolds number, R, of about 1.7×10^5. The drag coefficients, C_{ds}, derived from such tests are defined as

$$C_{ds} = \frac{F_d}{\frac{1}{2} D \rho U^2} \tag{36}$$

where F_d is the steady-state average drag force per unit of cylinder length and U is the steady flow velocity past the cylinder. The Reynolds number is

$$R = \frac{UD}{\nu} \tag{37}$$

where ν is the kinematic viscosity of the fluid.

14

EXPERIMENTS

Most of the data presented herein are from references (3,11). However, limited results from the experiments reported in (18) will also be shown. A detailed review of the experiments can be found in those references and only a very brief review will be given here to acquaint the reader with the general aspects of the work.

Equipment

The Wave Research Laboratory (WRL) at OSU is a flume 12 feet wide, 15 feet deep (of which 3.5 feet is freeboard), and 340 feet long. The test length that is relatively free of the evanescent effects from boundary conditions is about 126 feet long. A longitudinal section of the facility is shown in Fig. 5. Horizontal cylinders were towed from a carriage as indicated in Fig. 6 for determining the steady-state drag coefficient, C_{ds}, of the 8.625-inch diameter cylinders. Periodic waves were produced with periods ranging from 2.0 s to 6.0 s. The wave heights (trough-to-crest) were limited by incipient breaking up to a period of 2.6 s, where the wave height was about 5 feet. For periods greater than 2.6 s the maximum wave heights were limited by either the still water free board (3.5 feet) or the available energy from the wave generator (150 H.P.). The maximum height for the 6.0 s waves was 3 feet. Wave spectra were also produced, but the results therefrom will not be reported on herein. More details of the WRL and wave generation capabilities and characteristics can be found in (4,8,9).

The vertical 12.75-inch smooth aluminum cylinder (5) had a 12-inch long local force transducer that responded to the wave forces in a measurable way that was completely independent from the deflections, strains, and stresses

15

within the total cylinder structure. The vertical cylinder spanned smoothly from the wave flume floor to a beam 15 feet overhead, with no intermediate supports. The total forces and local pressures were also measured, but they will not be reported on here.

The vertical 8.625-inch diameter aluminum cylinder (11,12) also spanned from the wave flume floor to the overhead beam 15 feet above. However, it was necessary to provide intermediate supports at about 3.13 feet and 12.50 feet above the floor by means of small diameter, high strength guys that extended from the cylinder to the wave flume walls. The center of the local force transducer was at the same level as that for the 12.75-inch cylinder (3.7 feet below still water surface). However, the local forces were measured on a 2-foot long section. The transducer was constructed in such a way (11) that deflections of the support column could introduce a 13% influence on the measurements of local force in the in-line forces. (The transverse forces were influenced only 4%.) However, this influence was accurately quantified during calibrations by loading the entire cylinder as well as the local force transducer. (Similar calibration procedures proved that the local force readings were independent of support column strains for the 12.75-inch cylinder.) Experiments with this equipment were also performed on a sand-roughened cylinder that had a relative roughness, ϵ/D, of .023, where ϵ is the average maximum height of the sand grains, which were first determined with a sieve analysis, and later corroborated with circumferential measurements. Some of these results will be presented here to illustrate analysis techniques.

The water surface profile was measured with a sonic profiler embedded in the beam that provided the top support for the cylinders. The water velocities were measured for each cylinder with Marsh McBirney current meters

16

placed midway between the vertical cylinder and the wave flume walls, and at the same elevation as the center of the local force transducers (3.7 feet below the still water surface).

Measurements and Recording

Most measurement signals were recorded, filtered and unfiltered, wherein the filter was a Rockland 2-pole, low-pass filter with the cutoff frequency set at 8 Hz. The wave profiler was not filtered because of spurious results that would result from sharp 'spikes' or 'dropouts' that are inherent with sonic profilers and steep waves. Such records were filtered digitally. The current meter data were filtered in their own conditioning circuitry prior to the Rockland filter. Data processing included a calculation of the proper phase of each signal with the individual transfer functions so that the final smoothed signals were all properly phased with the water surface profile (3).

Signals were digitized at 256 increments per wave period. After complete processing, the data were reduced to 32 increments per wave, from which C_d, C_m, and other quantities, such as plotted information, were calculated. This information was stored on magnetic tape. For the 12.75-inch cylinder, data from 10 waves were recorded for each run, from which 7 peak-to-peak waves were defined. For most of the 8.625-inch diameter cylinder runs, 4 waves were recorded, from which 3 peak-to-peak waves were defined. Extra runs were made for the 12.75-inch diameter cylinder. Most of the processing for those runs was done on 3 or 4 waves from the 10 waves recorded in order to save data reduction costs.

It will be of interest to consider the results of some experiments made with a 12.75-inch diameter smooth cylinder (18) wherein the cylinder was oscillated horizontally in otherwise still water at a distance of 6 diameters

17

from the smooth bottom boundary and the still water surface. The apparatus was not constructed as well as for the vertical cylinders, so the results have considerable scatter. However, calibrations were carefully done and the central tendencies of the data trends are of considerable interest because Reynolds number of up to 7×10^5 were achieved, as well as Keulegan-Carpenter numbers up to 63.

DATA ANALYSIS AND RESULTS

Water Kinematics and Dynamics

Although water velocities can be measured with current meters, it is not possible to measure the accelerations directly. They were, therefore, calculated from the velocity measurements. Basically, the time derivative of the velocity measurements must be made to obtain the accelerations. The noise in the velocity measurements is then amplified for the accelerations. Calculating the derivative in the time domain yielded unacceptable results, even after time-domain filtering and inverse phase shifting. However, a frequency-domain procedure was developed by performing a Fourier transform of the velocity measurement, applying a transfer function based on linear wave theory to obtain the acceleration spectrum, setting to zero the energies above a frequency of 1.0 Hz, and performing the inverse Fourier transform to obtain the acceleration in the time domain. The resulting acceleration is smoothed of high frequencies and is theoretically properly phased with the velocities. The procedure is reviewed in detail in (5). However, the author thinks there are inaccuracies in the magnitude and phase of the accelerations of an unknown amount due to innate inaccuracies in the velocity measurements. There is also scatter in the phase of the accelerations so determined for a reason that is as yet unknown.

In this section the kinematics and dynamics of the water particles will be reviewed. A brief review of the rms errors between the measured kinematics and the stream function theory appears in (10). Generally, the values ranged from .10 to .28. This is a rigorous criterion because the rms error, E, is based on the velocity <u>vector</u>. That is,

$$\text{rms } E = \{\frac{1}{N} \sum_1^N [(u_m - u_\psi)^2 + (w_m - w_\psi)^2]_i\}^{1/2} / u_{\mu m} \tag{38}$$

where the subscript, m, is the measured value, and ψ is the value from stream function theory for the horizontal velocity, u, and the vertical velocity, w. Three somewhat typical results from kinematic measurements appear in Figs. 7, 8, and 9.

The phase shift of the acceleration, ϕ_a (see Fig. 4) can be predicted from stream function theory. Values of ϕ_a within the range of these experiments are plotted as the solid lines in Fig. 10, as a function of the wave height, H, and period, T. In addition, values were computed from the velocity measurements for the runs for the 12.75-inch cylinder. Each run had one value for each of the 7 waves measured. The average values of these for each run are also plotted in Fig. 10. The results show only rough agreement. It is concluded that errors in velocity measurements, even though they may be small, are amplifed considerably when accelerations are calculated therefrom. This is particularly true for the phase of the positive peak of the accelerations. Therefore, for the remainder of the analyses, it was decided to rely on the phase of the accelerations as determined from stream function theory.

In a closed system wave flume there is mass transport from the wave generator toward the beach in the general region above the wave troughs. This must be balanced by a return flow from the beach toward the wave generator, possibly at some depths below the troughs. The return flow was calculated by Kim (6) using Stokes fifth order wave theory and by assuming the return flow is uniform from the bottom of the flume up to the still water level. The return flow was also calculated from the kinematics measurements and the averages from a limited set of data are shown in Fig. 11. [They are also shown in a different way in (10).]

A broad agreement can be detected between measurements and theory. There is still considerable scatter, which is due to measurement errors and the fact that $\bar{u}$ is probably a function of time, whereas the theory is based on steady-state conditions. For the analyses herein $\bar{u}$ was determined from Fig. 11 and vectorially added to u from the stream function theory for analytical purposes here needed.

Phase Shift, $\hat{\phi}$, Normalized With 90°

It is desired to compare the different methods for determining $\hat{\phi}$. This was done for a cylinder uniformly coated with sand, such that the relative roughness, ε/D, was .023. The cylinder is designated as the SRC.02 and the phase was determined by the peak-to-peak method, the crossings method (average of the zero upcrossings and zero downcrossings), and the cross-correlation method. In each case the normalizing value used was 90°. This was done in an early phase of this work and was reported in (13). It is repeated here for completeness in order to compare the results of the different methods used on one cylinder. The SRC.02 (Sand Roughened Cylinder, k/D = .023) was also selected for this comparison because the results should be more influenced by the velocity (drag effects) than for the smooth cylinders.

These results for the SRC.02 are shown in Fig. 12. They show fairly tight plots for the zero crossings method and the cross-correlation method. The peak-to-peak method has more scatter, particularly at the higher K values. Figure 12 shows clearly that the $\hat{\phi}$ values are lowest for the peak-to-peak method, highest for the zero crossings method, and in-between for the cross-correlation method. These relationships are to be expected since velocities are low at the crossings, highest in the crest region, and averaged out for the cross-correlation method. Since the crest region of the wave is of

most interest and since the maximum force coefficient is determined from the maximum value of the force and the maximum velocity, the peak-to-peak method will be emphasized in the remaining part of this paper.

The 12.75-inch cylinder will henceforth be designated as the VSMC12 (Vertical Smooth Cylinder) and the 8.625-inch cylinder as the VSMC8. Selected runs for the VSMC12 were analyzed for $\hat{\phi}$ by using the cross-correlation and cross-spectrum analyses. The results are shown in Fig. 13. In fact, for a given K, the two methods were practically equal, though not identical. The data points were purposefully displaced in order to show for which points both analyses were made. Figure 14 shows the results for the zero crossings method. The phase, ϕ_f, is evidently smoothly changing from 1.0 to smaller values at a K of 15.

The results from the peak-to-peak method of finding $\hat{\phi}$ are shown in Fig. 15. The dashed line was constructed first for the VSMC12 alone, then for the VSMC8. The two curves were close, so an average was struck, which is represented by the dashed line up to about K = 20. The remainder of the line was drawn, taking into account the scatter from the horizontal 12.75-inch diameter cylinder (HSMC12). Obviously, more data are needed in the range 20 < K < 200.

Maximum Force Coefficient

The maximum force coefficient, C_μ, for the VSMC12 is shown in Fig. 16 wherein the value of u_μ is from the measured kinematics. Figure 17 shows the same information using u_μ as determined from the stream function theory. There is a little less scatter, particularly for K < 10, for the data based on stream function kinematics than for those based on the measured kinematics. Hence, it was decided to show most of the remaining data based on stream function kinematics wherever possible. Actually, even the seemingly small

22

scatter in Fig. 17 can be reduced further, as shown, approximately according
to β. The A line roughly represents the data for the larger β values and the
B line roughly represents the data for the smaller β values. It was seen in
(13) that C_μ vs. K data can be organized quite well for very rough cylinders,
and it was assumed at that time that they collapsed to a single line for
smooth cylinders. However, the carefully plotted information in Fig. 17 shows
that smooth cylinder data may be further organized according to β even for the
higher values of β.

It is also of interest to note that for small K Eq. (25) can be expressed
accurately with only the second term. Then, taking

$$\hat{F}_\mu = C_\mu = \frac{\pi^2 C_m}{K} \tag{39}$$

it can be seen that the slope of the plot in Fig. 17 should be -1, which is
nearly the case.

Figure 18 is the similar plot for the VSMC8. The β breakdown is indi-
cated and it appears to be close to that for Fig. 17. That is, the A and B
lines fall nearly at the same positions.

However, C_μ for higher values of K are needed to show how C_μ varies for
all values, knowing that it should approach C_{ds} as K gets large, according to
Eq. (31). Some approximate data were obtained from the experiment records
that were accomplished for (18). Plots for the VSMC12, VSMC8, and the HSMC12
are summarized in Fig. 19. From these data it seems to be reasonable to use
the curves as drawn to approximate the relation of C_μ to K for all values of
K. Of course, these are tentative curves that need to be verified with addi-
tional data at high K values from any valid available source. The value of
C_{ds} in the figures is the average of several tow tests made with the smooth

23

aluminum 8.625-inch diameter cylinders up to R values of 7×10^5. The values ranged between .4 and .6.

It is of interest to note that it _may_ be possible, as indicated in Fig. 19, that C_μ can be determined at laboratory scales for all values of K if the high values are determined from C_{ds} and the low values are up to high enough K so that $C_\mu \simeq C_{ds}$. This also implies for all values of R! It will be seen shortly that the same is not true for $\hat{\phi}$ or $\tilde{\phi}$.

Phase Shift, $\tilde{\phi}$, Normalized With ϕ_a

Attention is now directed toward $\tilde{\phi}$ to see for what values of K the force record is nearly in phase with the velocity record (drag-dependent). Figure 10 shows that as K increases (i.e., as H and/or T increase), ϕ_a gets smaller. It turns out that $\tilde{\phi}$ from Eq. (4) remains quite high because although the maximum force becomes more closely in phase with u, the phase of $\dot{u}$ also moves toward that of u, so that $\tilde{\phi}$ reduces only slowly, as shown in Fig. 20. Since ϕ_a is dependent on measured values of H and T, there is considerably more scatter in $\tilde{\phi}$. Thus, the forces measured were heavily dominated by the acceleration effects up to K values even as high as 23.

Drag and Inertia Coefficients

The normalized phase, $\hat{\phi}$, is plotted for the VSMC12, VSMC8, and the HSMC12 in Fig. 15. This figure and Fig. 19, along with Eqs. (32) and (35), were used to obtain values of C_d and C_m that would yield best approximations of the magnitude of the maximum force.

The values of C_d and C_m are shown in Fig. 21, where the smooth curves are from Eqs. (32), (33), and (35), using the smooth curve values of C_μ and ϕf determined from Figs. 15 and 19. The plotted points in Fig. 21 are the values

24

of C_d and C_m determined from the respective cylinders, as calculated with least squares methods (5) and averaged over a minimum of three waves in any run, and up to seven in some.

It is possible that the scatter in data values of C_d and C_m in Fig. 21 can be further organized according to broad ranges of R and β. Actually, data indicate C_μ can be organized according to β, when plotted as a function of R. Equations (32) and (35) can be transformed to functions of R and β through $K = R/β$. So, this further refinement, or organization of the scatter according to β, is left for a future effort.

25a

CONCLUSIONS

- The relative phase shifts between the maximum velocity, the maximum measured force, and the maximum acceleration show immediately whether a wave and cylinder diameter arrangement will produce conditions that are acceleration- (inertia) or velocity- (drag) dependent. Up to a K of at least 25, the local wave force on a smooth vertical cylinder is heavily dependent on the fluid acceleration.

- A plot of the maximum force coefficient, C_μ, vs. K, the Keulegan-Carpenter number, can be generated for all K (which implies for all R) with waves at least as large as those produced in the Oregon State University Wave Research Laboratory, in conjunction with steady tow tests at Reynolds number at least well beyond the critical value (up to about 7×10^5).

- Laboratory results are mostly limited from determining accurate values of the _phase_ of the force measurement, ϕ_f, at higher K values. Data plots of $\hat{\phi}$ vs. K, up to a K of from 25 to 60, indicate that the force is _still strongly influenced by the acceleration_ (inertia) effects. Only for roughened cylinders can laboratory results at OSU show dominant drag conditions at higher K values.

SUGGESTIONS FOR FUTURE STUDIES

- The _total_ in-line force acting on the VSMC12 cylinder can be determined from existing measurement data. The phase of the total force should not necessarily be the same as that of the local measured force because the drag term in the Morison equation has its greatest influence in the region between the wave trough and crest. The phases of the top and bottom reactions (both were measured) can be determined analytically using the local force measurement as a benchmark. Thus the measured and analytical phases of the total force with respect to the local force can be compared. It is possible that the total force will be more influenced by the drag effects because the Keulegan-Carpenter number is higher in the trough-to-crest region.

- It is possible that the _transverse_ force measurements can be organized with respect to a maximum force coefficient concept in conjunction with the phase of the transverse force. This can probably be accomplished with spectrum analysis techniques. These measurements and analyses could be compared to the 8 local pressure measurements for verification.

- Maximum force coefficient and phase angle can be utilized for organizing the random wave forces. The Keulegan-Carpenter number can be associated with the frequency and spectrum amplitudes and the maximum force coefficient can be related to the velocity and force spectra. The C_μ and $\hat{\phi}$ can probably be well represented as functions of wave frequency. The influence of nonlinearities may introduce problems, but a linear assumption could be made as a first approximation. Values of C_d and C_m obtained in this manner can be compared to values obtained by a conventional wave-by-wave analysis.

27

ACKNOWLEDGEMENTS

REFERENCES

1. Chakrabarti, S., "Hydrodynamic Coefficients and Depth Parameter," Journal of Waterway, Port, Coastal and Ocean Division, A.S.C.E., Vol. 111, No. 1, January 1985.

2. Dean, R.G., "Methodology for Evaluating Suitability of Wave and Wave Force Data for Determining Drag and Inertia Coefficients," Proceedings of First International Conference on Behavior of Offshore Structures, Trondheim, Norway, [BOSS '76], August 1976.

3. Heidemann, J.C., Olsen, O.A., and Johansson, P.I., "Local Wave Force Coefficients," Proceedings of the Specialty Conference Civil Engineering in the Oceans IV of the American Society of Civil Engineers, San Francisco, California, September 1979.

4. Hudspeth, R.T., Jones, D.H., and Nath, J.H., "Analyses of Hinged Wave-makers for Random Waves," Proceedings of the 16th International Conference of Coastal Engineering, Hamburg, Germany, August and September 1978.

5. Hudspeth, R.T. and Nath, J.H., "High Reynolds Number Wave Force Investigation in a Wave Flume, Vol. I," Final Report to NCEL and MMS, Dept. of Civil Engineering, Oregon State University, February 1984.

6. Kim, T.I., "Mass Transport in Laboratory Water Wave Flumes," Ph.D. thesis, Department of Civil Engineering, Oregon State University, June 1985.

7. Morison, J.R., O'Brien, M.P., Johnson, J.W., and Schaaf, S.A., "The Force Exerted by Surface Waves on Piles," Petroleum Transactions, AIME, Vol. 150, 1950, pp. 149-154.

8. Nath, J.H. and Kobune, K., "Periodic Theory Velocity Prediction in Random Waves," Proceedings of 16th International Conference of Coastal Engineering, Hamburg, Germany, August and September 1978.

9. Nath, J.H. (with an Appendix by M.S. Longuet-Higgins), "Drift Speed of Buoys in Waves," Proceedings of the 16th International Conference of Coastal Engineering, Hamburg, Germany, August and September 1978.

10. Nath, J.H., "Heavily Roughened Horizontal Cylinders in Waves," Specialty Conference on Behavior of Offshore Structures, Massachusetts Institute of Technology, [BOSS '82], August 1982.

11. Nath, J.H., "Hydrodynamic Coefficients for Cylinders with Pronounced Marine Growths, API PRAC Project 80-31B - Vertical Cylinder," Final Report to American Petroleum Institute, Dept. of Civil Engineering, Oregon State University, January 1983.

12. Nath, J.H., "Vertical vs. Horizontal Cylinders in Waves," Proceedings of Specialty Conference on Pipelines in Adverse Environments, ASCE, San Diego, California, November 1983.

13. Nath, J.H., Hsu, M-K, Hudspeth, R.T., and Dummer, J., "Laboratory Wave Forces on Vertical Cylinders," Proceedings of Specialty Conference on Ocean Structural Dynamics Symposium '84, Oregon State University, September 1984.

14. Sarpkaya, T., and Isaacson, M., Mechanics of Wave Forces on Offshore Structures, Van Nostrand Reinhold Co., 1981.

15. Sarpkaya, T., Discussion for "Quasi-2-D Forces on a Vertical Cylinder in Waves," Waterway, Port, Coastal and Ocean Engineering Division Journal of ASCE, February 1983, by Stansby, T.K., Bullock, G.N., and Short, I. Discussion is in same journal, February 1984.

16. Stansby, P.K., Bullock, G.N., and Short, I., "Quasi-2-D Forces on a Vertical Cylinder in Waves," Journal of Waterway, Port, Coastal and Ocean Division, A.S.C.E., Vol 109, No. 1, February 1983.

17. Starsmore, N., "Consistent Drag and Added Mass Coefficients From Full Scale Data," OTC3990, Proceedings of the Offshore Technology Conference, Houston, Texas, May 1981.

18. Yamamoto, T. and Nath, J.H., "High Reynolds Number Oscillating Flow by Cylinders," Proceedings of the 15th International Conference of Coastal Engineering, Hawaii, July 1976.
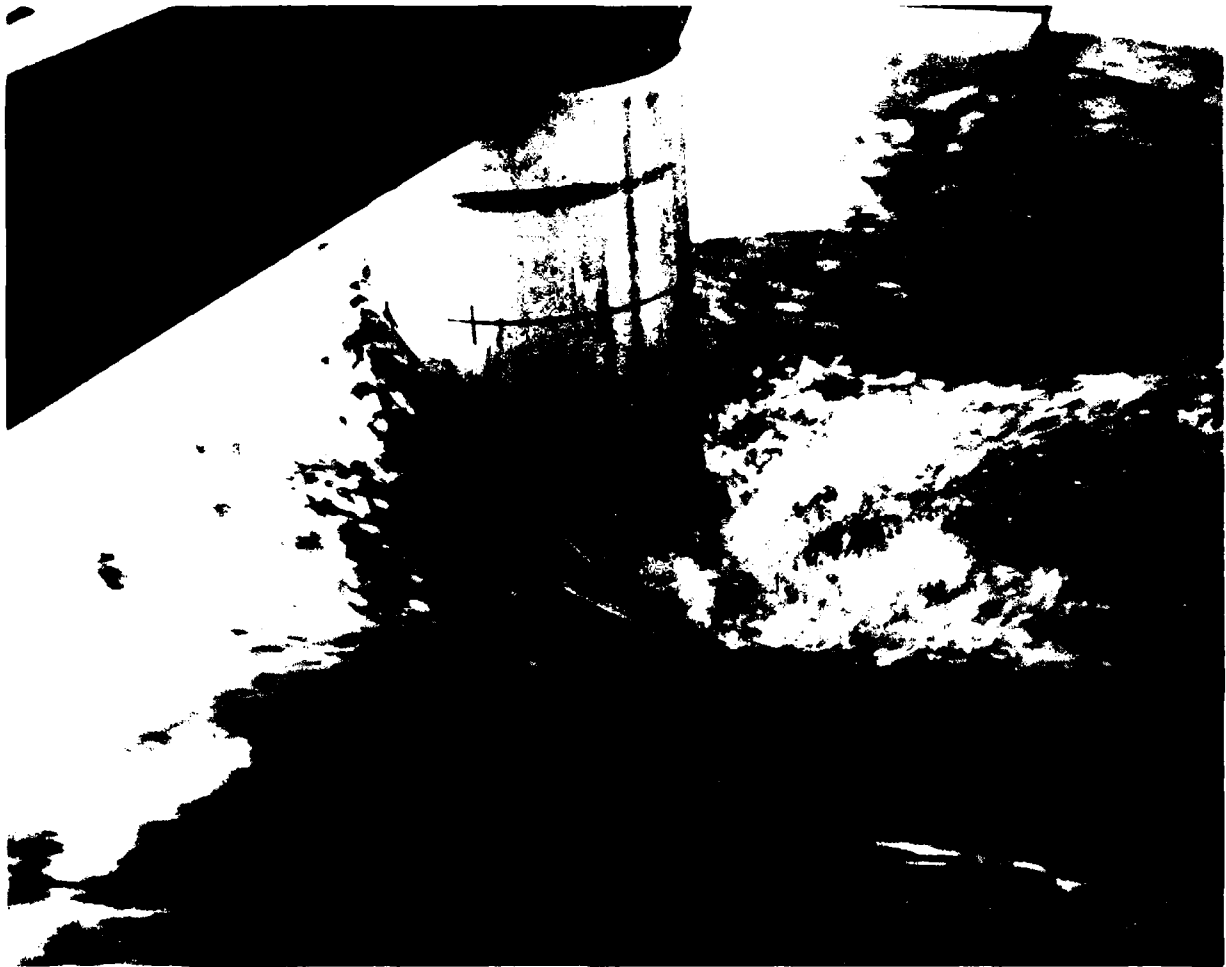
Fig.1.-Runup at the crest of a laboratory wave on
a 12.75-inch diameter smooth vertical cylinder.
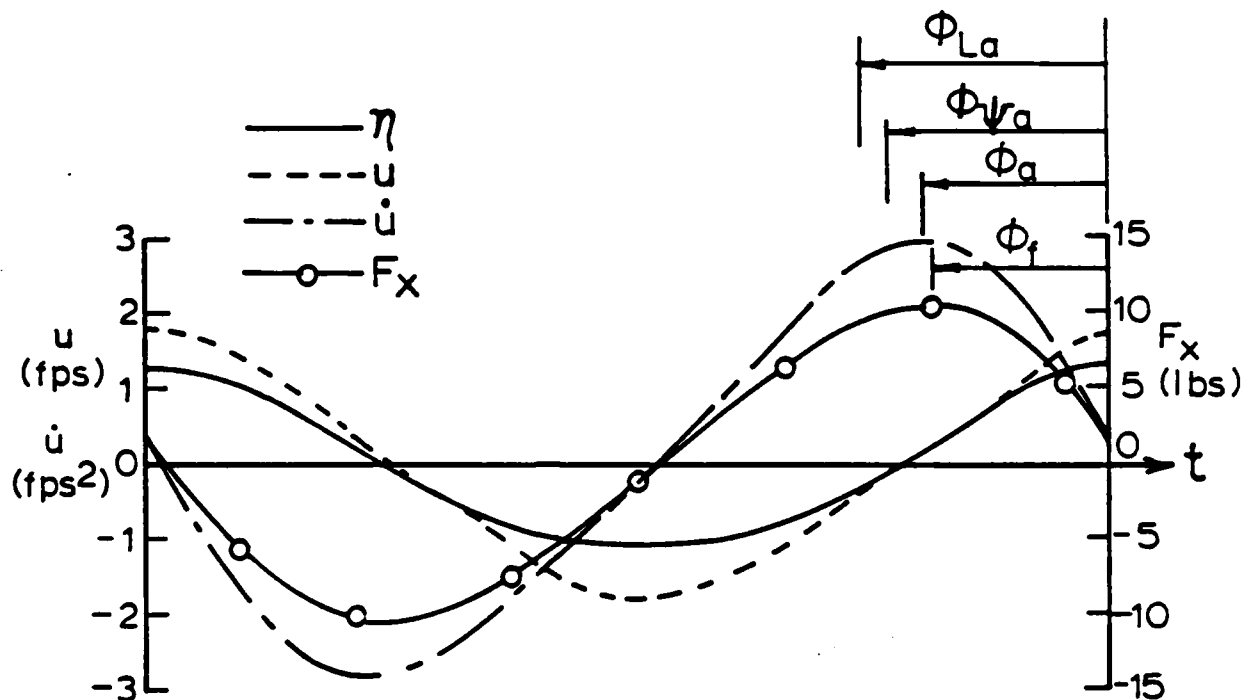
Fig. 2.-Local horizontal force, velocity and acceleration for 12.75"
smooth vertical cylinder. T = 3.7s, H = 2.39 ft., K = 6.3, R = 1.4x10^5.
ϕ_{La} and $\phi_{\psi a}$ = acceleration phase shift from linear and stream function
theories, respectively.
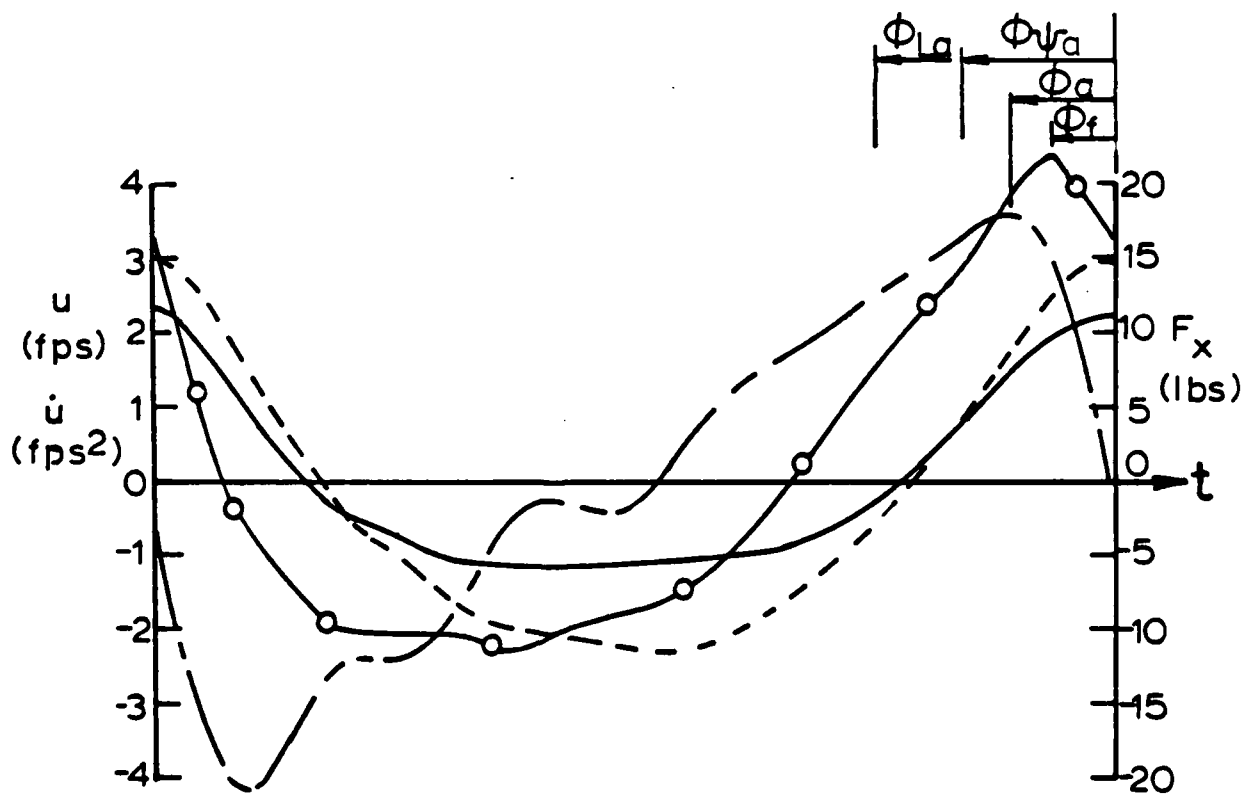
Fig. 3.-Local horizontal force, velocity and acceleration for 8.625"
SRC.02 vertical cylinder. T = 5.29s, H = 3.46 ft., K = 21.6, R =
1.5x10^5. ϕ_{La} and $\phi_{\psi a}$ = acceleration phase shift from linear and
stream function theories, respectively.
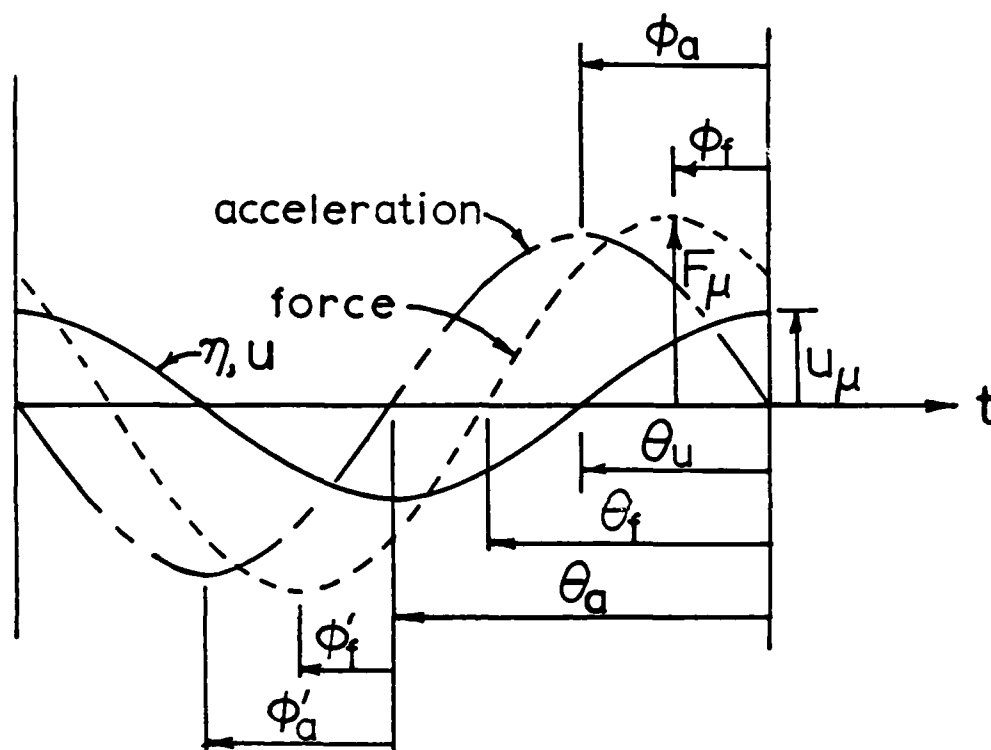
Fig. 4.-Definition sketch for the phases and magnitudes
of the velocity, acceleration, and local force measurements
on a vertical cylinder in a periodic wave.

PLAN
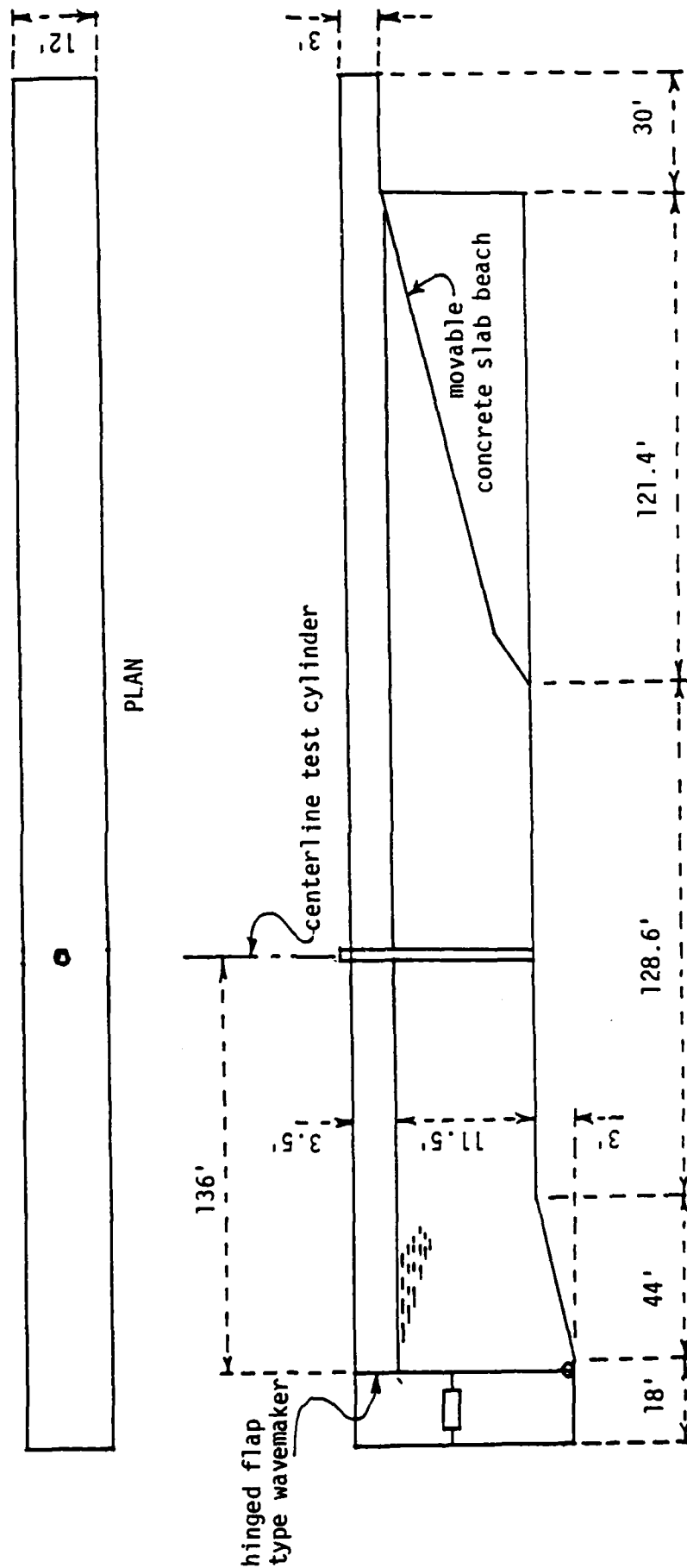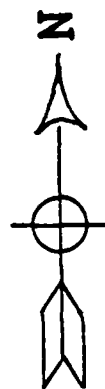
Fig. 5.- OSU Wave Flume

34
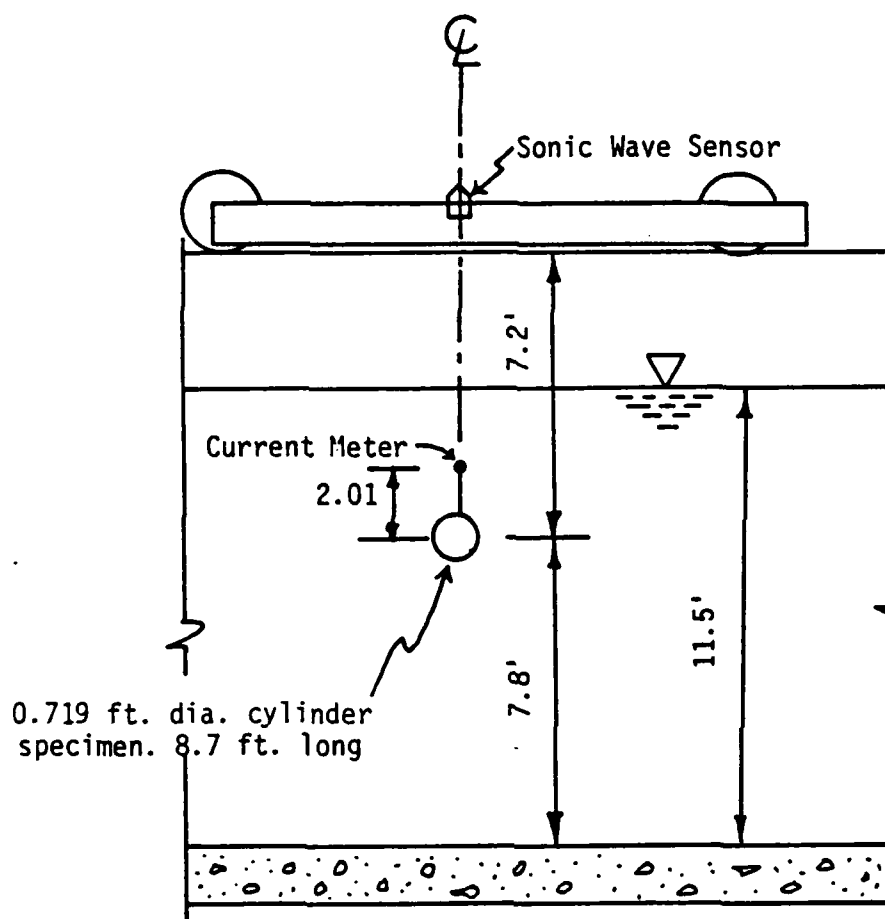
Fig.6.-Tow carriage arrangement for determining C_{ds} for the horizontal cylinders.

RUN T25H37.005   T=2.5   H=3.25
HORIZONTAL VELOCITY COMPARISON
$\bar{u}$ = -.20 fps

o   MEASURED DATA
.   LINEAR WAVE THEORY
x   STREAM FUNCTION THEORY
$\bar{u}$ = time averaged velocity measurement near
    the wall, in line with the center of the
    force transducer

X AXIS IS PHASE IN DEGREES

Fig. 7.- Horizontal velocity comparisons for wave #2 of run #5

36

RUN T46H31.029   T=4.6   H=3.57
HORIZONTAL VELOCITY COMPARISON

ō   MEASURED DATA   ū = -.11 fps
.   LINEAR WAVE THEORY
×   STREAM FUNCTION THEORY

ū = time averaged velocity measurement
    near the wall, in line with the
    center of the force transducer
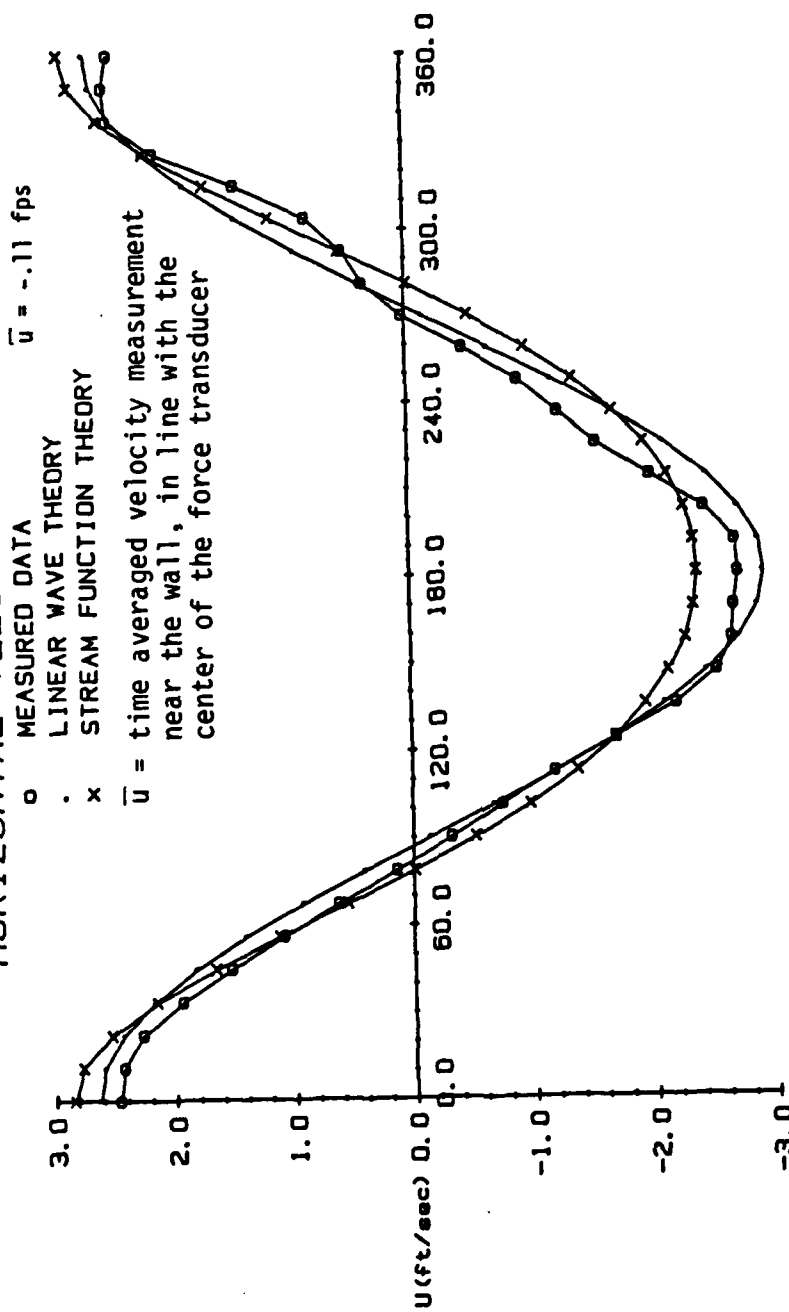
X AXIS IS PHASE IN DEGREES

Fig. 8.-   Horizontal velocity comparisons for wave #2 of run #29

37

RUN T60H33.020   T=6.0   H=2.78
HORIZONTAL VELOCITY COMPARISON   ū = -.15 fps

o   MEASURED DATA
.   LINEAR WAVE THEORY
x   STREAM FUNCTION THEORY

ū = time averaged velocity measurement
near the wall, in line with the
center of the force transducer
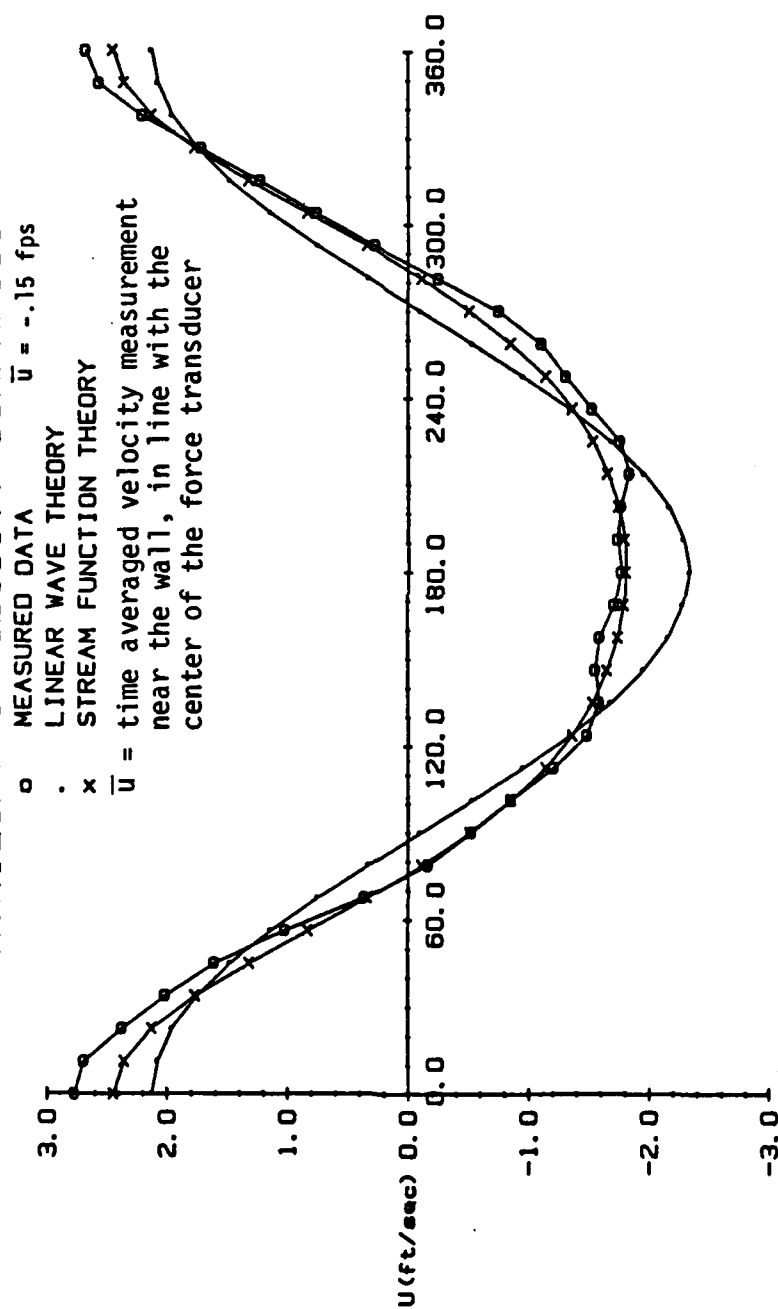
X AXIS IS PHASE IN DEGREES

Fig. 9.-   Horizontal velocity comparisons for wave #2 of run #20

38
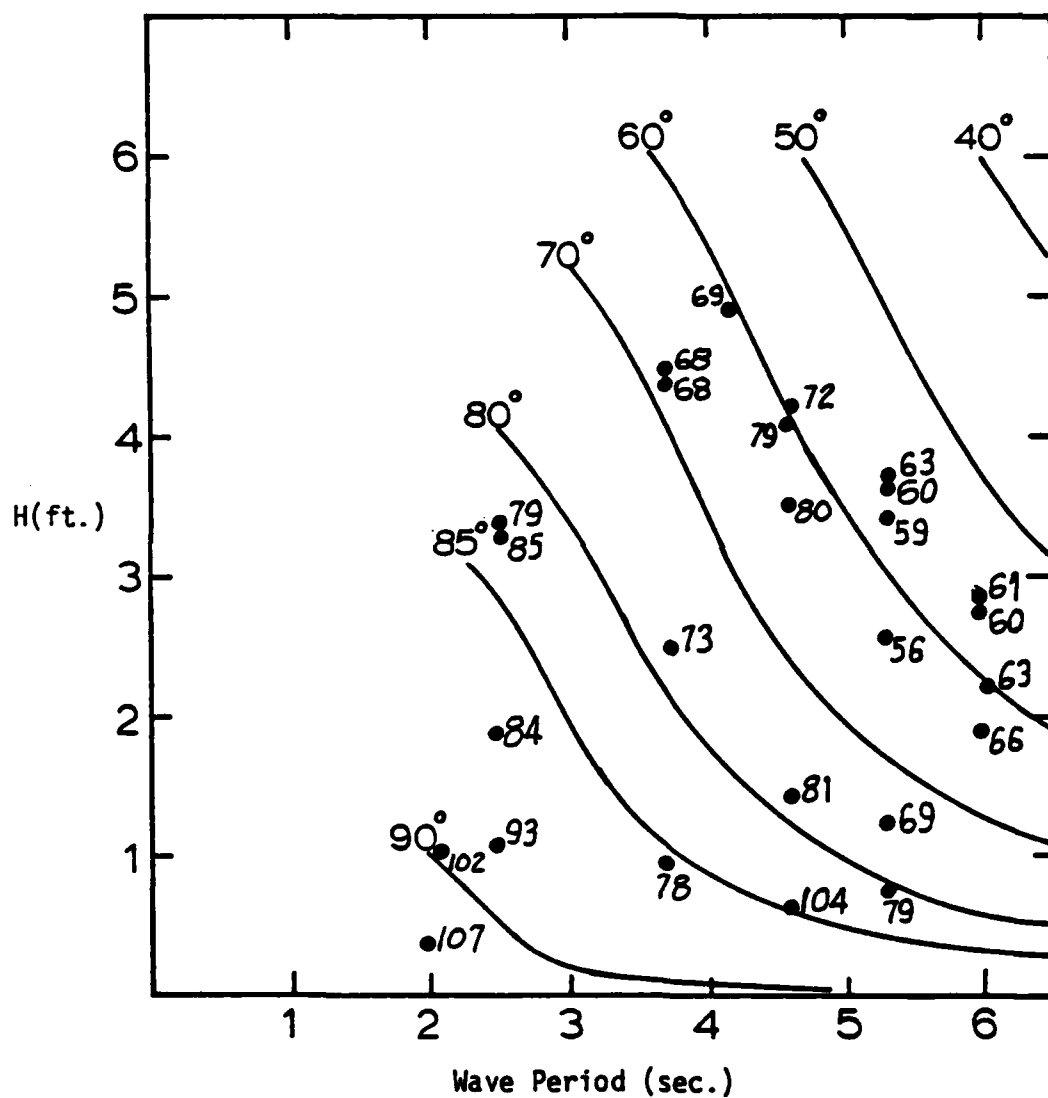
Fig.10.- Phase in degrees of the acceleration peaks with respect to
the velocity peaks (negative values). Stream function
theory for periodic waves (————) vs. data (·) (average of
7 waves). Water depth = 11.5 ft., depth below surface =
3.7 ft. (Data from 12.75-inch vertical cylinder tests of
April, 1983)
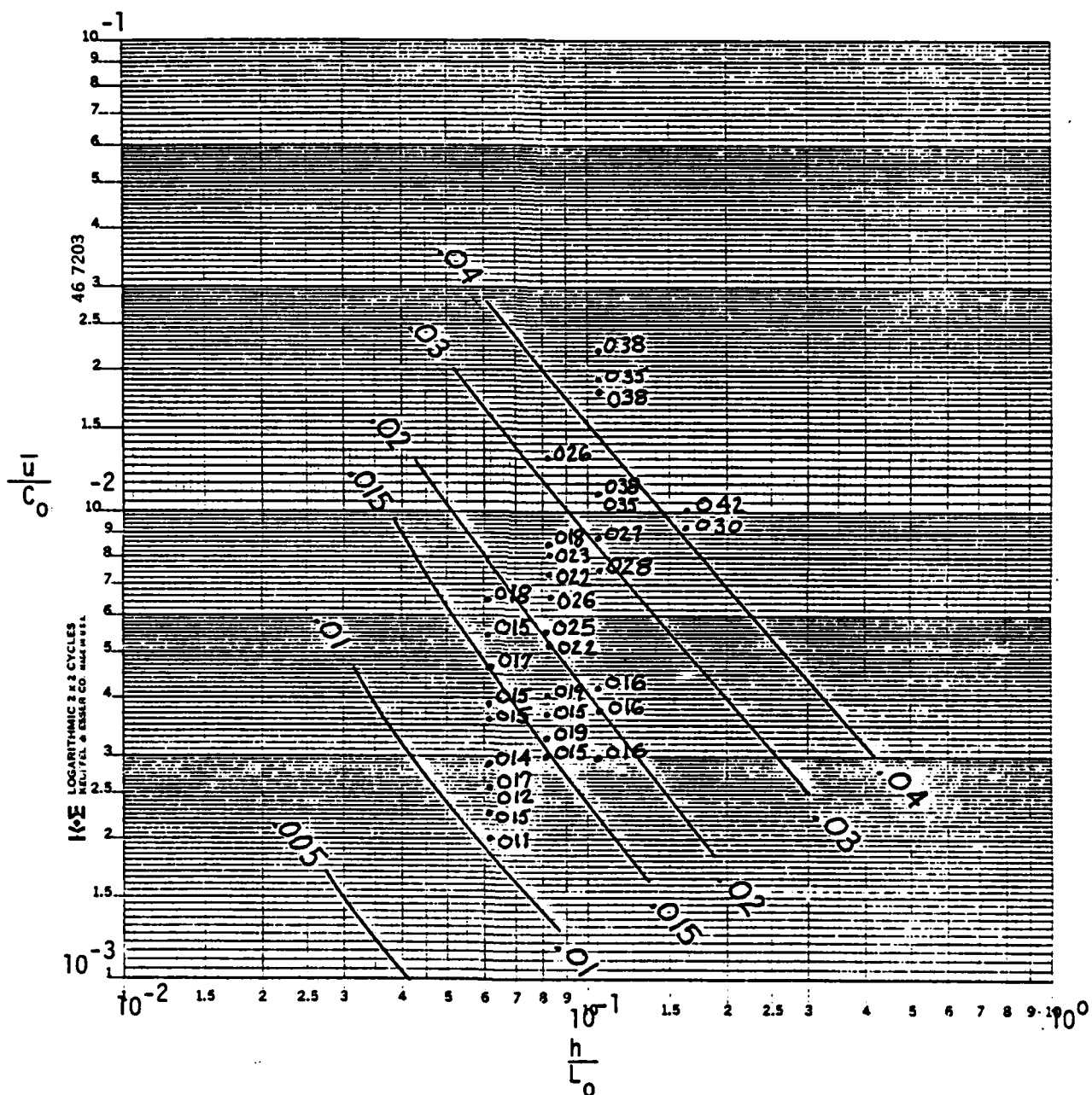
Fig. 11 Values of H/L_0, where $L_0 = 5.12 \ T^2$, $C_0 = L_0/T$, h = water depth, $\bar{u}$ = return flow (negative, toward waveboard);

————— = theoretical values from Stokes 5th order wave theory (5); numbers = experimental values, where the decimal point is also the data plot point.
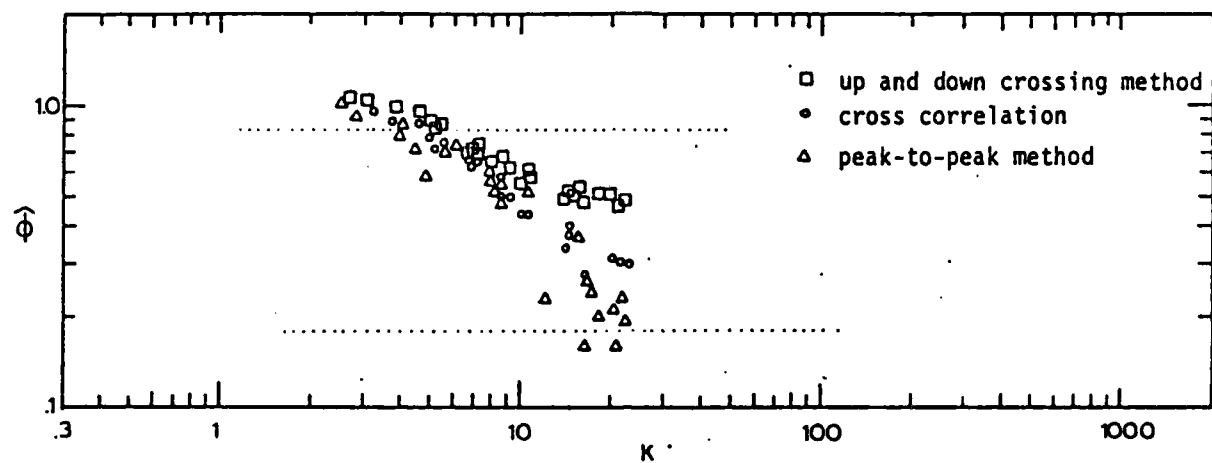
Fig. 12 Phase shift for the VSRC.02
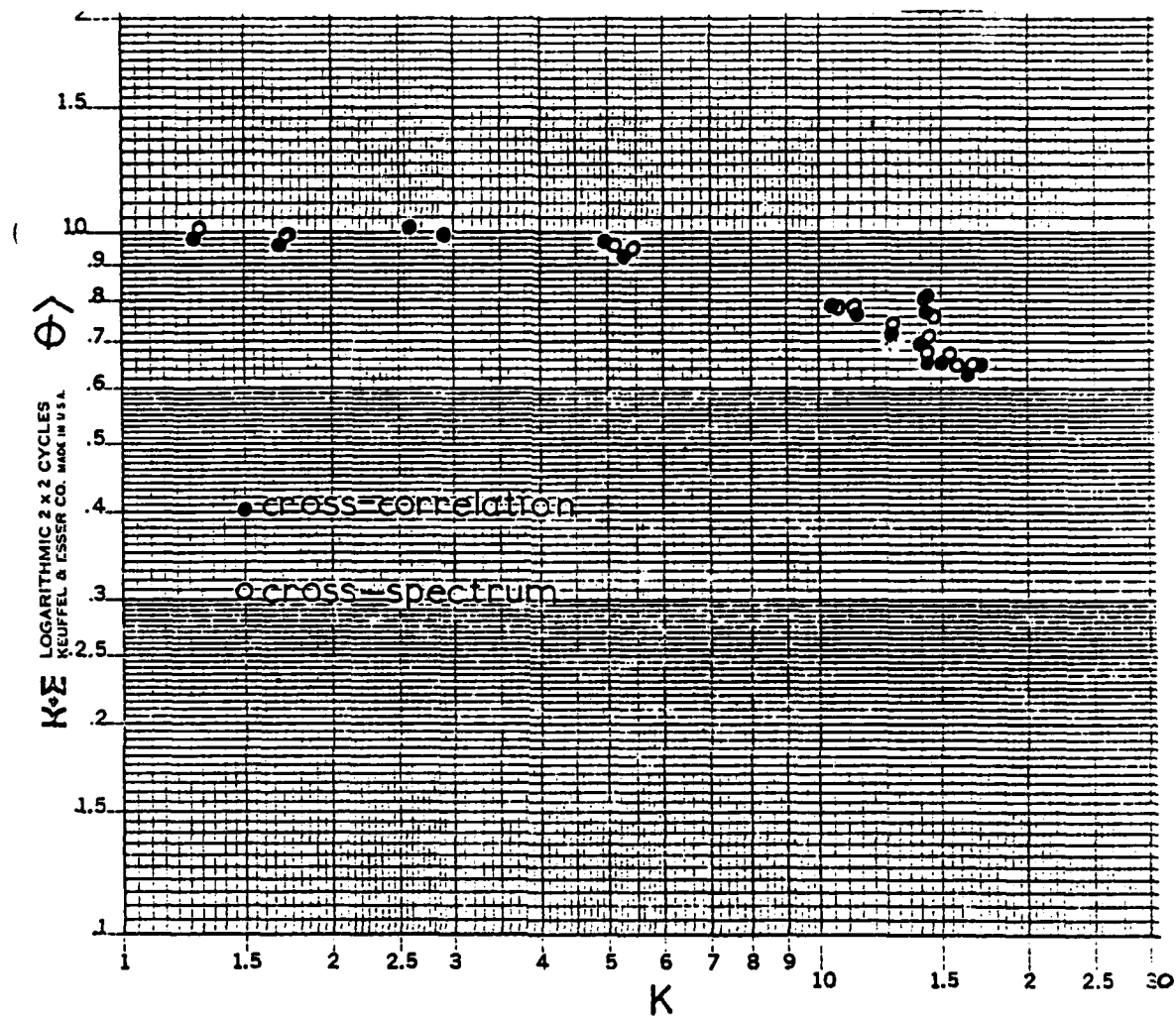
Fig. 13.-Normalized phase shift, $\hat{\phi}$, as determined by cross-correlation and cross-spectrum analyses (two waves analyzed per run)
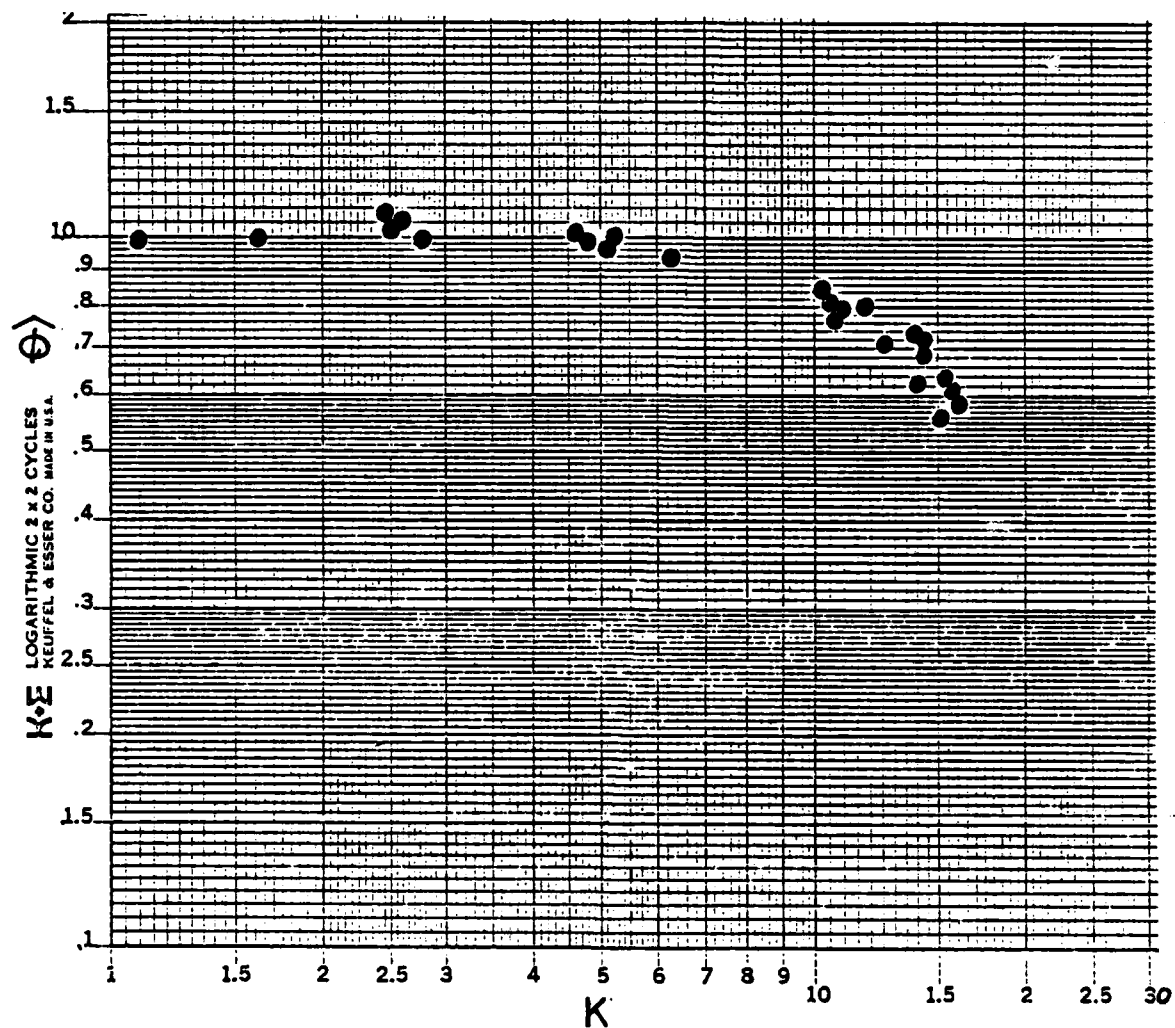
Fig. 14.-Normalized phase shift, $\hat{\phi}$, as determined by averaging the phases at the upcrossings and downcrossings. (Six waves analyzed per run)
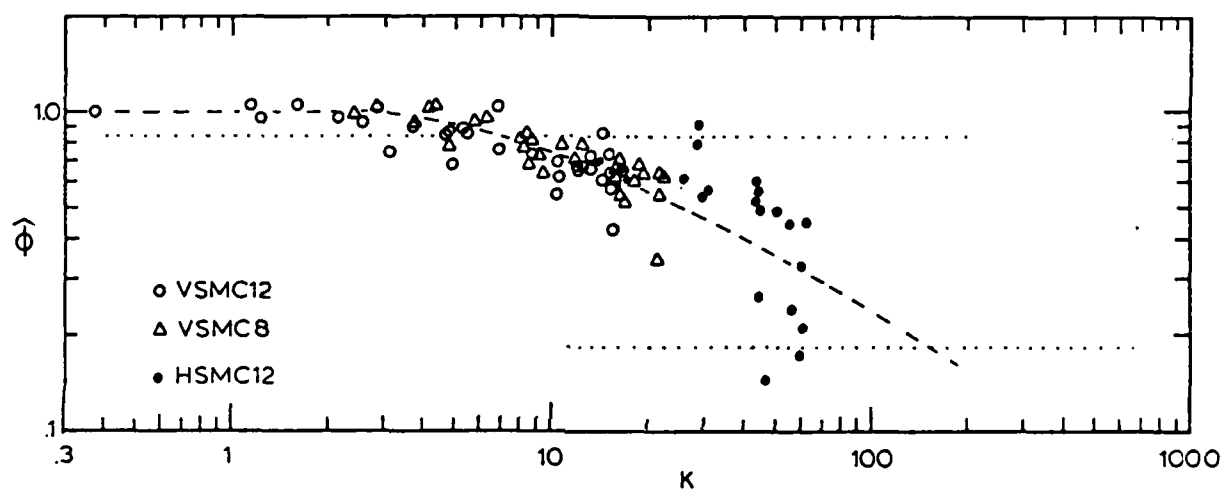
Fig. 15.-Normalized phase shift, $\hat{\phi}$, as determined by the peak-to-peak method for the VSMC12, VSMC8 and HSMC12 constructions. (Various numbers of waves analyzed for each run)
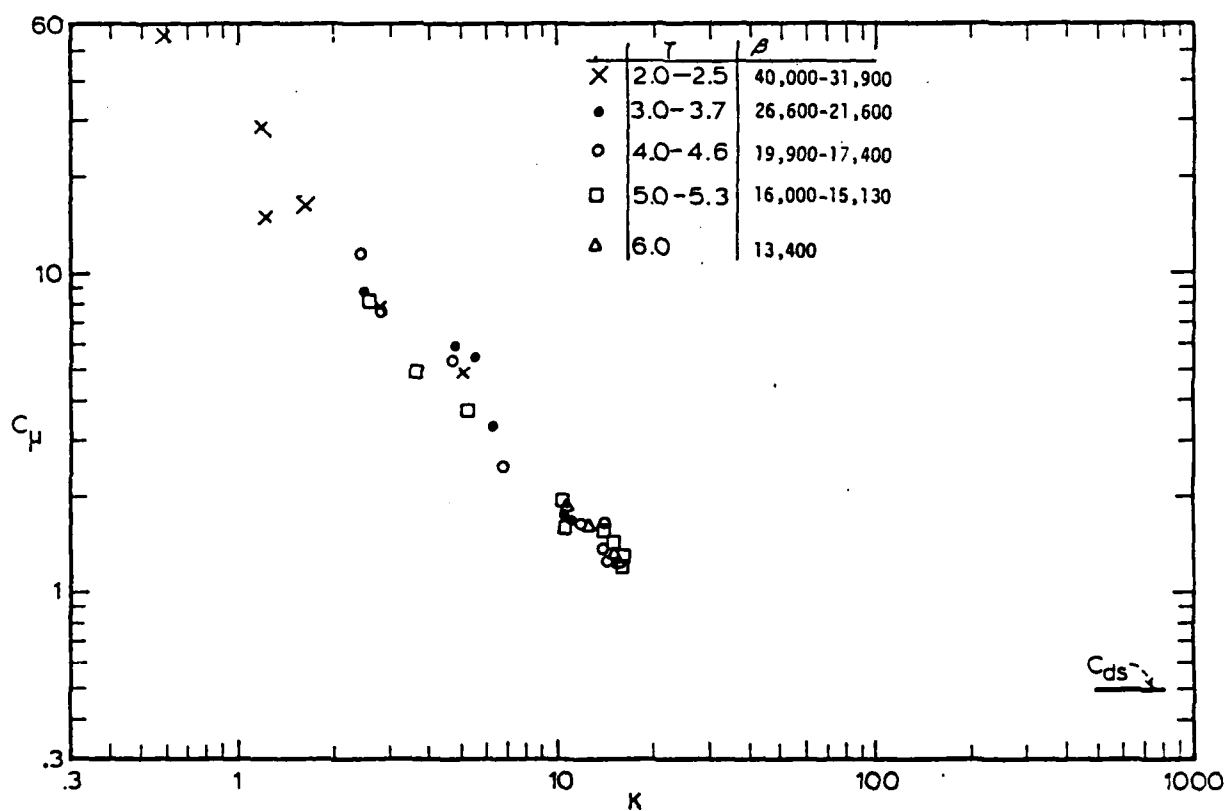
Fig.16.-Maximum force coefficients for the VSMC12 specimen, using measured kinematics for u_μ.
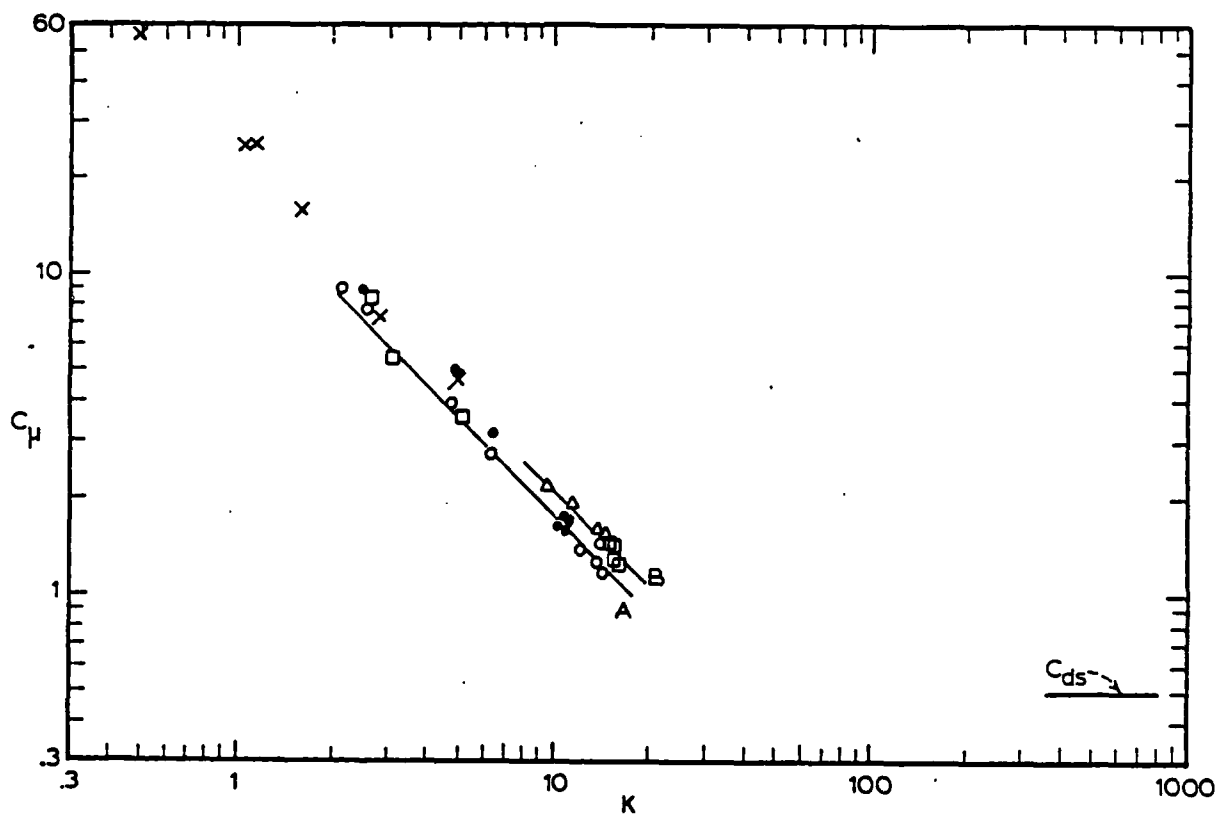
Fig. 17.-Maximum force coefficient for the VSMC12, using stream
function kinematics. See Fig. 16 for legend. Line A is approximately
in the range 17000<β<27000. Line B is approximately in the range
13400<β<17000.
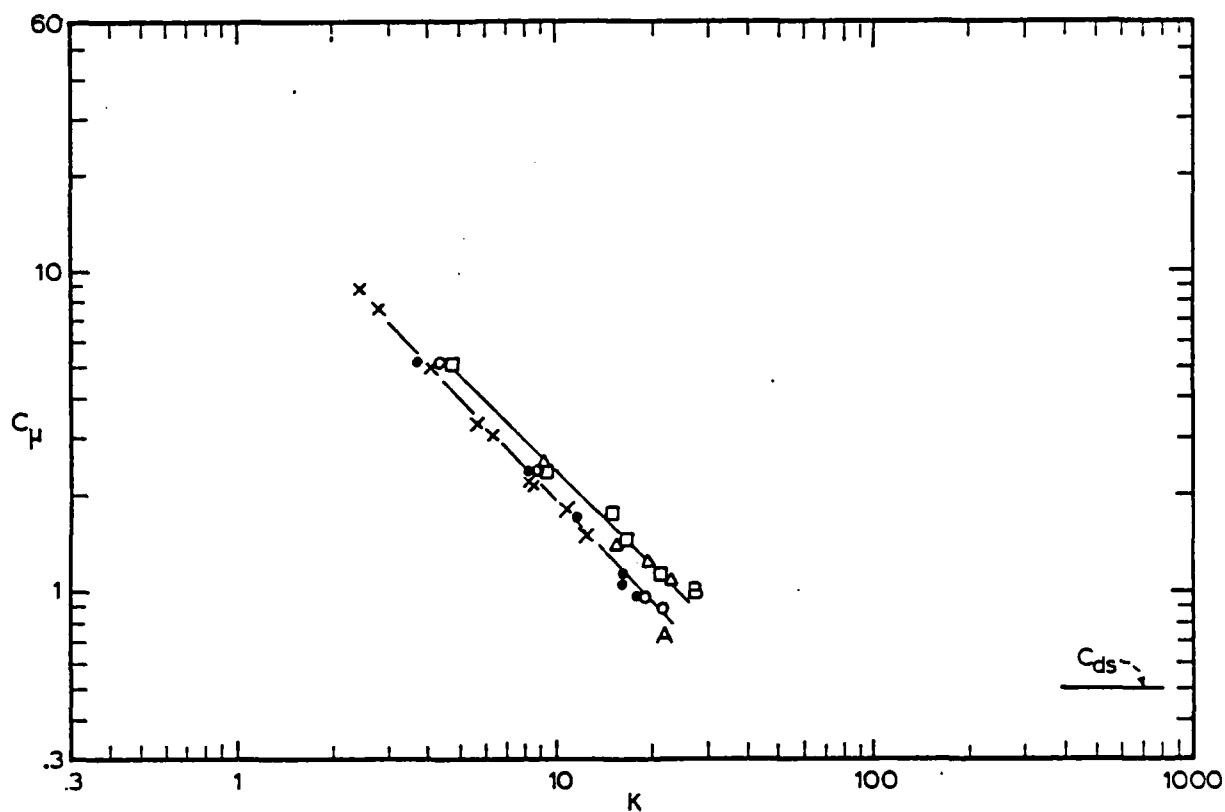
Fig. 18.-Maximum force coefficient for the VSMC8, using stream function kinematics. See Fig. 16 for legend. Line A is approximately in the range 17000<β<27000. Line B is approximately in the range 13400<β<17000.
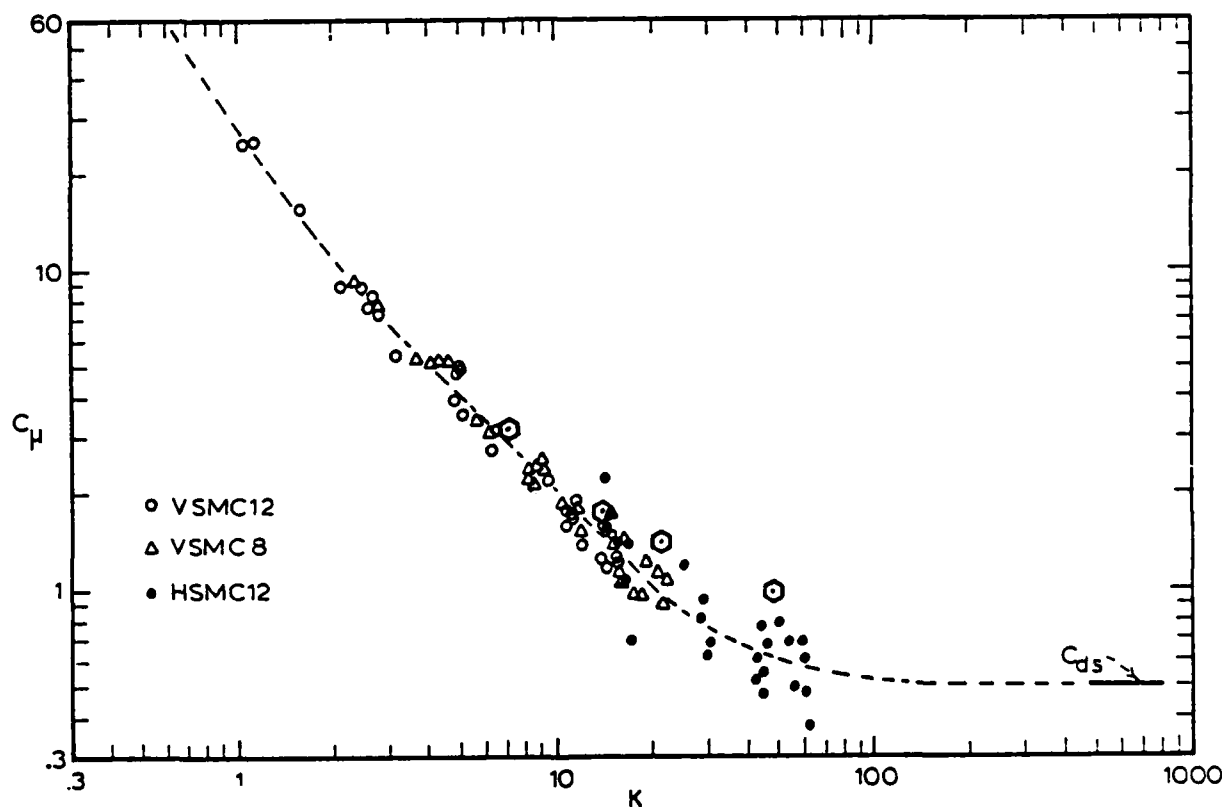
Fig. 19.-Maximum force coefficients for the VSMC12, VSMC8, and the HSMC12, superimposed without regard to β.

⊙ represents data transposed from ref. (1) at the mid-range of the scatter for 4 selected values of K, assuming sinusoidal velocity and force measurements. (In the reference the K and C_μ items were based on rms values.) Note that $C_\mu \to 1.0$ in ref.(1) as K gets large, which indicates the results behave like those for a roughened cylinder.
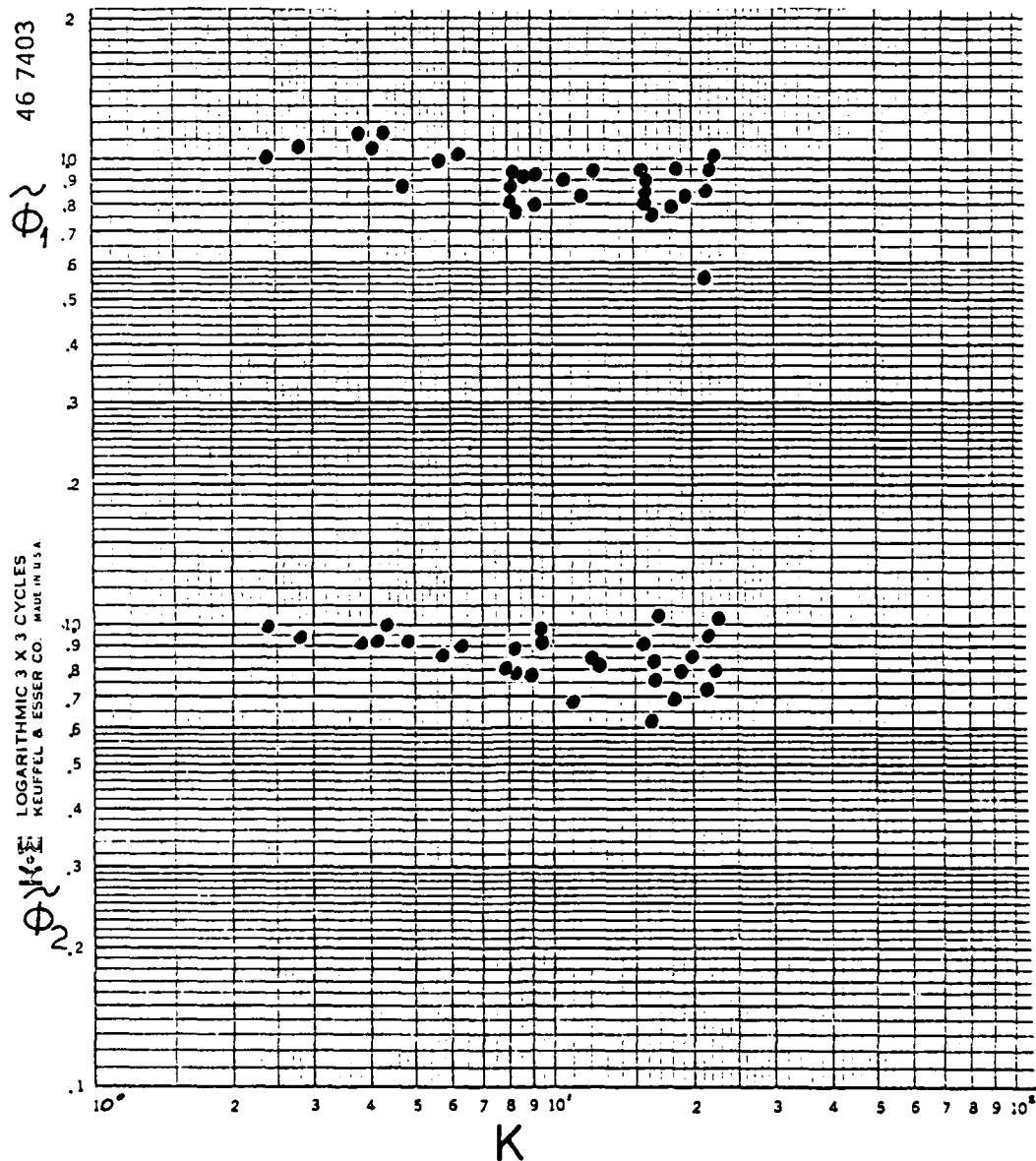
Fig. 20.-Normalized phase shift, $\tilde{\phi}$, using the stream function dynamics for $\tilde{\phi}_1$ and the 'measured' ϕ_a for $\tilde{\phi}_2$.
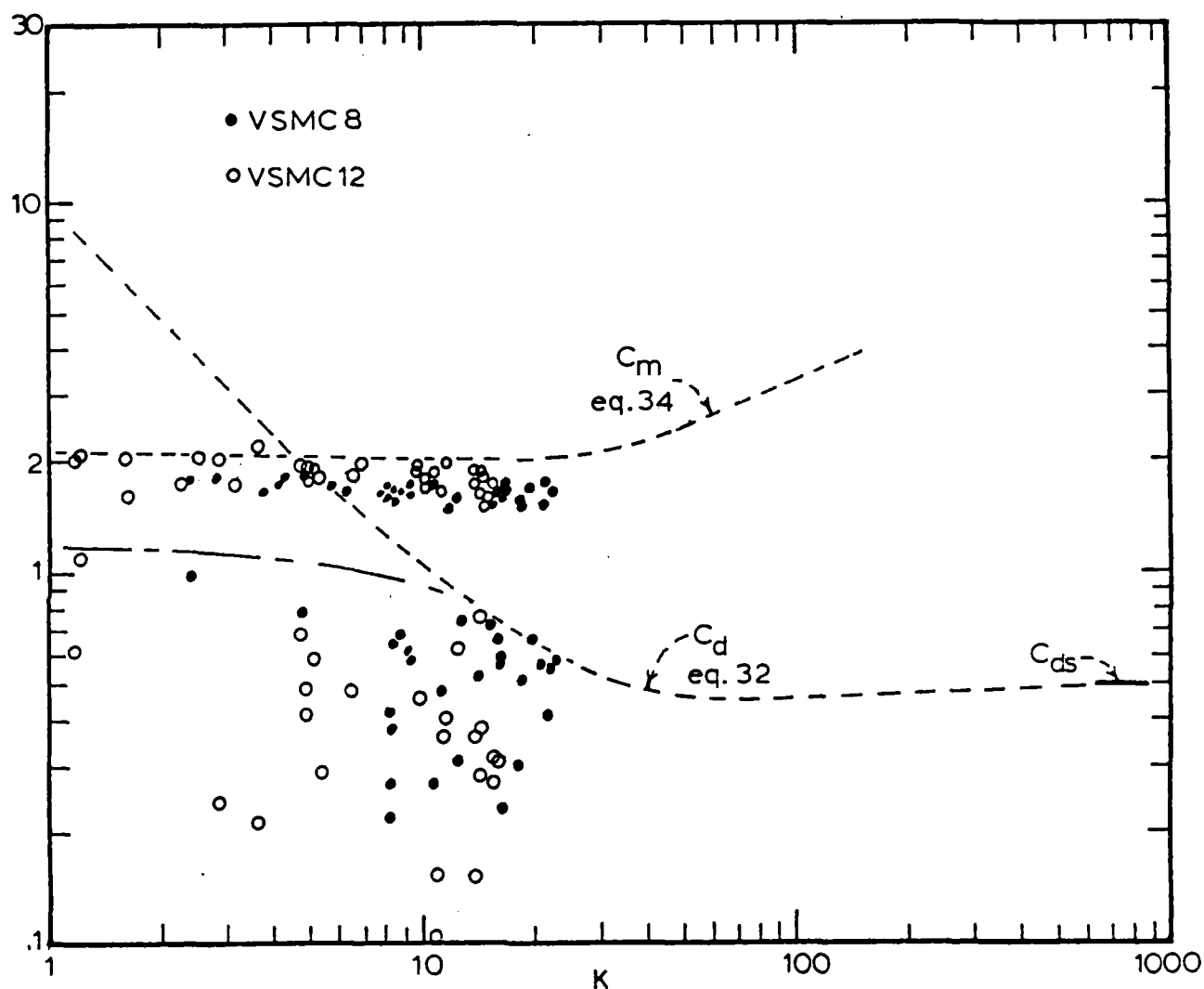
Fig.21.-Values of C_d and C_m from Eqs. (32) and (34), using the curves shown in Figs. 15 and 19. The data points are the least squares values of C_d and C_m for the VSMC12 and VSMC8 cylinders.

50a

APPENDIX

NCEL 12" Vertical Cylinder Smooth

Re & K based on Measured kinematics

$\hat{\phi} = \phi_f/\phi_a$ 7 wave average except where noted

$$\overline{\hat{\phi}}$$

ϕ_a	Run #	T (secs)	$\overline{H}$ (ft)	$\overline{K}$	$\overline{Re} \times 10^{-5}$	Peak	Trough	Cross Correlation	(up+down)/2	$\overline{C_M}$
102.1[1]	1	2.00	1.07	1.15	0.46	.86	1.08	.98	1.03	29.42
106.9[2]	2	2.00	0.35	0.37	0.15	.86	1.15	.97	.98	94.34
93.3[3]	3	2.50	1.01	1.60	0.51	.94	1.09	1.03	.94	16.81
83.6	4	2.50	1.88	2.85	0.91	1.02	1.00	1.02	1.03	7.90
...[5]	5	3.70	2.29	5.35	1.71	.88	.96	.98	1.02	6.21
78[6]	6	3.70	0.94	2.55	0.55	1.08	.97	1.02	1.01	8.61
73.1	7	3.70	2.52	6.81	1.47	.91	.99	.97	.98	3.36
67.5	28	3.70	4.40	12.19	2.64	.87	.93	.84	.79	1.81
104.5	9	4.60	0.63	2.19	0.38	.85	1.06	.97	.98	10.67
81.2	10	4.60	1.41	4.88	0.85	.96	.90	.98	1.01	5.19
80.4	29	4.60	3.53	12.46	2.17	.77	.89	.86	.84	1.65
72.4 or 78.8	12	4.60	4.17	15.43	2.69	.98	.92	.85	.78	1.46
78.8	13	5.30	0.76	3.04	0.46	.86	.98	.97	1.01	7.69
69.1	14	5.30	1.22	4.89	0.74	.92	.96	.95	.98	3.68
56.3	15	5.30	2.57	10.27	1.55	.89	.96	.91	.87	1.96
58.7	16	5.30	3.42	14.28	2.16	.94	.90	.88	.66	1.58
57.5	17	5.30	3.66	15.29	2.31	.88	.88	.85	.64	1.47
65.9	30	6.00	1.90	8.73	1.16	.99	.98	.89	.84	1.77
62.7	31	6.00	2.28	10.48	1.40	.97	.97	.88	.79	1.56
61.1, 60.3	20	6.00	2.81	13.40	1.79	1.04	.97	.85	.80	1.34
69.1[1]	21	4.20	4.90	16.34	3.09	.79	.80	.78	.79	1.68
62.9	22	5.30	3.71	15.26	2.32	.97	.92	.85	.64	1.18
60.9 72.9[23]	23	4.60	4.16	14.80	2.58	.99	.96	.84	.74	1.25
67.5[4]	24	3.70	4.41	12.21	2.64	.92	.82	.87	.80	1.69
78.8[5]	25	2.50	3.38	5.52	1.77	.90	.93	.98	1.01	5.16
61.1, 60.3[6]	26	6.00	2.79	13.04	1.74	1.00	.96	.88	1.28	1.28
[27]	27	2.00	1.03	1.23	0.49	1.15	.88	1.00	.99	14.81
*[28]	37	3.00	2.45	4.69	1.25	1.02	.96	1.00	1.01	4.78
*[29]	39	4.00	0.91	2.82	0.56	.98	.99	.99	.99	7.36
*[30]	40	4.00	2.27	6.88	1.38	.95	.96	.95	.9?	2.60

* 3 wave average

JDR 12/5/84

NCEL 12" Vertical Cylinder (Smooth)

3 wave average except where noted — $\overset{\rightarrow}{\hat{\phi}}$ JDR 12/5/84

	Run #	T (sec)[2]	$\overline{H}$ (ft)[3]	$\overline{K}$ [4]	$\overline{Re} \times 10^{-5}$ [5]	Peak[6]	Trough	Cross Correlation	(up+down)/2	C_M
1	42	5.00	0.73	3.63	0.58	.96	.98	.95	.96	4.81
2	43	5.00	2.80	10.68	1.71	.84	1.03	.89	1.03	1.59
3	44	5.00	4.32	15.32	2.45	.80	.87	.81	.78	1.35
*4	45	3.00	4.51	8.53	2.28	.75	.77	.92	.93	2.96
5						.				
6	* one wave									
7										
8										
9										
10										
11										
12										
13										
14										
15										
16										
17										
18										
19										
20										
21										
22										
23										
24										
25										
26										
27										
28										
29										
30										

45-385

National

NCEL 12" Vertical Smooth Cylinder

$$C_M = \frac{F_M}{\frac{1}{2} D U^2 L} \qquad \tfrac{1}{8}$$

D = 12¾" ρ = 1.94 lbm/ft³
L = 1 ft

Run #	Wave #	F_{MM}	U_{MM}	C_M^5	C_M^6 Average	K_M^7/K_V	U_{MM}^8	C_M^9	Average C_M
1	1	6.36	.46	29.16			.53	22.0	
	2	5.71	.44	28.62			.46	26.2	
	3	5.84	.41	33.71			.46	26.8	
	4	5.93	.44	29.72			.47	26.0	
	5	5.83	.45	27.93			.48	24.6	
	6	5.91	.48	24.89			.48	24.9	
	7	5.90	.43	30.96	29.28	1.19/1.15	.48	24.8	25.0
2	1	2.04	.17	68.49			.17	68.5	
	2	1.99	.13	114.25			.16	75.4	
	3	1.98	.13	113.68			.16	75.0	
	4	2.04	.17	68.49			.17	68.5	
	5	1.99	.15	85.82			.16	75.4	
	6	1.98	.14	98.02			.16	75.0	
	7	2.01	.18	60.19	86.99	.39/.37	.16	76.2	.73.4
3	1	5.69	.63	13.91			.62	14.4	
	2	5.54	.57	16.54			.58	16.0	
	3	5.77	.58	16.64			.59	16.1	
	4	5.60	.56	17.33			.58	16.2	
	5	5.69	.53	19.65			.58	16.4	
	6	5.68	.60	15.31			.59	15.8	
	7	5.67	.60	15.28	16.38	1.62/1.59	.60	15.3	15.7
4	1	10.07	1.14	7.52			1.15	7.39	
	2	10.15	1.08	8.44			1.20	6.84	
	3	10.26	1.11	8.08			1.13	7.80	
	4	10.35	1.15	7.59			1.11	8.15	
	5	10.20	1.12	7.89			1.17	7.23	
	6	10.18	1.14	7.60			1.17	7.22	
	7	10.19	1.11	8.02	7.88	2.77/2.81	1.20	6.87	7.36

JDR 1/2/85

NCEL 12" Vertical Smooth Cylinder

	Run #	Wave #	F_M [3]	U_M [4]	C_M [5]	C_M [6]	$\overline{K_M}/\overline{K_V}$ (Average)	U_{vM} [8]	C_M [9]	Average C_M
1	5	1	16.86	1.63	6.16			1.78	5.16	
2		2	17.21	1.57	6.77			1.78	5.27	
3		3	17.53	1.64	6.32			1.84	5.02	
4		4	17.35	1.69	5.89			1.78	5.31	
5		5	17.43	1.58	6.77			1.86	4.89	
6		6	17.45	1.74	5.59			1.92	4.59	
7		7	17.41	1.96	4.40	5.99	4.80/4.99	1.92	4.58	4.98
8										
9	6	1	4.20	.65	9.65			.69	8.56	
10		2	4.43	.70	8.77			.61	11.6	
11		3	4.21	.70	8.34			.69	8.58	
12		4	4.14	.69	8.44			.69	8.44	
13		5	4.16	.72	7.79			.68	8.73	
14		6	4.12	.66	9.18			.70	8.16	
15		7	4.13	.63	10.10	8.90	2.50/2.50	.71	7.95	8.85
16										
17	7	1	10.47	1.81	3.10			1.73	3.39	
18		2	10.66	1.80	3.19			1.79	3.23	
19		3	11.07	1.78	3.39			1.76	3.47	
20		4	11.62	1.79	3.52			1.77	3.60	
21		5	11.40	1.85	3.23			2.08	2.56	
22		6	11.06	1.67	3.85			1.85	3.14	
23		7	11.08	1.84	3.18	3.35	6.28/6.50	2.00	2.69	3.15
24										
25	28	1	16.95	2.96	1.89			3.00	1.83	
26		2	16.14	2.93	1.82			3.08	1.65	
27		3	18.16	3.08	1.86			3.20	1.72	
28		4	17.27	3.33	1.51			3.27	1.57	
29		5	17.46	3.03	1.85			3.08	1.79	
30		6	17.73	3.24	1.64			3.15	1.73	
		7	18.63	3.11	1.87	1.77	10.7/10.9	3.17	1.80	1.73

JDR 1/2/85

	Run[1] #	Wave[2] #	F_M [3]	U_M [4]	C_M [5]	C_M [6]	Average $\overline{K_M}/\overline{K_V}$ [7]	U_{V_M} [8]	C_M [9]	Average C_M
1	9	1	2.31	.49	5.34			.46	10.6	
2		2	2.37	.39	15.11			.46	10.9	
3		3	2.25	.46	10.32			.46	10.3	
4		4	2.14	.39	13.65			.46	9.81	
5		5	1.98	.40	12.00			.51	7.39	
6		6	1.94	.45	9.26			.50	7.53	
7	*	7	1.91	.23	35.21	11.6	2.41/2.15	.55	6.12	8.95
8										
9	10	1	5.14	1.00	4.99			1.12	3.98	
10		2	5.15	.98	5.20			1.08	4.28	
11		3	5.19	.93	5.82			1.04	4.66	
12		4	4.95	.90	5.93			1.14	3.70	
13		5	4.75	.88	5.95			1.12	3.67	
14		6	5.01	1.03	4.58			1.16	3.61	
15		7	4.66	.87	5.97	5.49	4.59/4.82	1.11	3.67	3.94
16										
17	29	1	11.43	2.46	1.83			2.80	1.41	
18		2	11.71	2.49	1.83			2.82	1.43	
19		3	11.40	2.67	1.55			3.03	1.20	
20		4	11.09	2.67	1.51			2.84	1.33	
21		5	10.85	2.60	1.56			2.82	1.32	
22		6	10.47	2.55	1.56			2.68	1.41	
23		7	10.72	2.47	1.70	1.65	11.8/12.2	2.80	1.33	1.35
24										
25	12	1	13.31	2.88	1.56			3.17	1.29	
26		2	13.53	3.07	1.39			3.14	1.33	
27		3	13.81	3.17	1.33			3.38	1.17	
28		4	12.32	2.96	1.36			3.25	1.13	
29		5	12.68	3.15	1.24			3.10	1.28	
30		6	10.88	2.68	1.47			2.92	1.24	
		7	13.64	3.15	1.33	1.38	14.0/13.8	3.29	1.22	1.24

* Not included in the average

JDR 1/2/85

NCEL 12" Smooth Vertical Cylinder

	Run[1]#	Wave[2]#	F_M[3]	U_M[4]	C_M[5]	C_M[6]	$\overline{K_N}/\overline{K_V}$[7]	U_{VM}[8]	C_M[9]	Average C_M
1	13	1	2.30	.56	7.12			.58	6.63	
2		2	2.28	.52	8.18			.58	6.58	
3		3	2.14	.52	7.68			.61	5.58	
4		4	2.13	.50	8.27			.64	5.05	
5		5	1.99	.53	6.87			.65	4.57	
6		6	2.13	.44	10.68			.67	4.60	
7		7	2.21	.51	8.24	8.15	2.61/3.14	.67	4.78	5.40
8										
9	14	1	3.94	1.02	3.67			.98	3.98	
10		2	3.93	1.07	3.25			.99	3.79	
11		3	3.97	1.03	3.63			1.00	3.85	
12		4	3.94	1.12	3.05			1.05	3.47	
13		5	3.63	.95	3.90			1.07	3.08	
14		6	3.70	1.05	3.26			1.11	2.91	
15		7	4.20	.88	5.26	3.72	5.21/5.18	1.06	3.63	3.53
16										
17	15	1	8.35	2.09	1.85			2.19	1.69	
18		2	8.73	2.09	1.94			2.13	1.87	
19		3	8.88	2.14	1.88			2.21	1.76	
20		4	8.36	2.03	1.97			2.25	1.60	
21		5	9.11	2.07	2.06			2.34	1.61	
22		6	8.91	2.07	2.02			2.27	1.68	
23		7	9.06	2.09	2.01	1.96	10.4/11.2	2.32	1.63	1.69
24										
25	16	1	11.82	2.75	1.52			2.87	1.39	
26		2	13.50	2.82	1.65			2.90	1.56	
27		3	12.95	2.89	1.50			2.87	1.53	
28		4	13.17	2.89	1.53			2.94	1.49	
29		5	12.49	2.81	1.53			2.84	1.50	
30		6	11.66	2.57	1.71			2.88	1.36	
		7	12.77	2.68	1.73	1.60	14.0/14.3	2.76	1.63	1.49

JDR 1/2/85

NCEL 12" Vertical Smooth Cylinder

	Run #[1]	Wave #[2]	F_m[3]	V_m[4]	C_m[5]	C_m[6]	$\bar{K}_n/\bar{K}_v$[7]	U_{vm}[8]	C_m[9]	Average C_m
1	17	1	13.58	2.99	1.47			3.09	1.38	
2		2	14.68	3.14	1.44			3.15	1.44	
3		3	14.08	3.19	1.34			2.98	1.54	
4		4	12.75	2.93	1.44			3.15	1.25	
5		5	13.48	3.01	1.44			3.16	1.31	
6		6	13.38	2.93	1.51			3.17	1.29	
7		7	13.83	3.09	1.41	1.44	15.1/15.3	2.83	1.68	1.41
8										
9	30	1	6.12	1.83	1.77			1.77	1.90	
10		2	6.45	1.99	1.58			1.68	2.22	
11		3	6.44	1.80	1.93			1.62	2.38	
12		4	6.04	1.76	1.89			1.67	2.10	
13		5	6.47	1.96	1.63			1.61	2.42	
14		6	6.63	1.86	1.86			1.73	2.15	
15		7	6.74	1.89	1.83	1.90	10.7/9.57	1.77	2.09	2.18
16										
17	31	1	8.06	2.17	1.66			2.10	1.77	
18		2	7.86	2.22	1.55			2.10	1.73	
19		3	8.28	2.34	1.47			2.03	1.95	
20		4	7.83	2.28	1.46			2.05	1.81	
21		5	7.75	2.24	1.50			2.04	1.81	
22		6	7.96	2.13	1.70			2.02	2.07	
23		7	8.30	2.03	1.95	1.61	12.6/11.6	2.05	2.12	1.89
24										
25	20	1	9.73	2.78	1.22			2.61	1.39	
26		2	9.97	2.67	1.36			2.45	1.61	
27		3	9.41	2.71	1.24			2.50	1.46	
28		4	9.77	2.81	1.20			2.59	1.41	
29		5	8.96	2.51	1.38			2.42	1.48	
30		6	9.78	2.38	1.68			2.43	1.61	
		7	10.23	2.63	1.44	1.36	15.1/14.0	2.29	1.89	1.55

JDR 1/2/85

45-38

National

NCEL 12" Vertical Smooth Cylinder

	Run[1]*	Wave[2]*	F_m[3]	U_m[4]	C_m[5]	C_m[6]	$\overline{K_m}/\overline{K_v}$[7]	$U_{y,m}$[8]	C_m[9]	Average C_m
1	21	1	20.76	3.30	1.85			3.45	1.69	
2		2	19.48	3.29	1.75			3.54	1.51	
3		3	20.68	3.41	1.73			3.70	1.47	
4		4	19.13	3.46	1.55			3.60	1.43	
5		5	20.03	3.44	1.64			3.62	1.48	
6		6	19.83	3.51	1.56			3.53	1.54	
7		7	20.96	3.54	1.62	1.67	14.1/14.1	3.51	1.65	1.54
8										
9	22	1	12.89	3.14	1.27			3.07	1.33	
10		2	12.55	3.14	1.24			3.14	1.24	
11		3	13.22	3.43	1.09			3.19	1.26	
12		4	12.72	3.37	1.09			2.95	1.42	
13		5	12.32	3.25	1.13			3.23	1.15	
14		6	12.45	3.13	1.23			3.25	1.14	
15		7	12.36	3.09	1.26	1.19	16.3/15.7	3.30	1.10	1.23
16										
17	23	1	13.32	3.07	1.37			3.39	1.12	
18		2	13.22	3.22	1.24			3.34	1.15	
19		3	13.73	3.19	1.31			3.42	1.14	
20		4	12.93	3.47	1.04			3.32	1.14	
21		5	12.74	3.10	1.29			3.15	1.25	
22		6	13.50	3.23	1.26			3.16	1.31	
23		7	12.54	3.06	1.30	1.26	14.3/14.3	3.27	1.14	1.18
24										
25	24	1	15.51	2.86	1.84			3.07	1.60	
26		2	16.96	3.15	1.66			3.08	1.73	
27		3	16.24	3.11	1.63			3.29	1.46	
28		4	17.17	3.07	1.77			3.16	1.67	
29		5	17.74	3.32	1.56			3.12	1.77	
30		6	16.05	3.17	1.55			3.14	1.58	
		7	16.47	3.06	1.71	1.67	11.0/11.0	2.13	*3.52	1.64

* Not included in the computation of the average

JDR 1/2/85

NCEL 12" Vertical Smooth Cylinder

	Run[1]#	Wave[2]#	F_M[3]	U_M[4]	C_M[5]	C_M[6]	Average $\overline{K_M}/\overline{K_Y}$	U_{wp}[8]	C_M[9]	Average C_M
1	25	1	17.11	1.86	4.80			1.85	4.85	
2		2	17.30	1.91	4.60			1.78	5.30	
3		3	17.28	1.64	6.23			1.85	4.89	
4		4	17.46	1.81	5.17			1.86	4.90	
5		5	17.17	1.78	5.26			1.89	4.66	
6		6	17.57	1.96	4.44			1.92	4.62	
7		7	17.13	1.93	4.46	4.99	5.10/5.12	1.99	4.20	4.78
8										
9	26	1	9.49	2.46	1.52			2.64	1.32	
10		2	9.36	2.89	1.09			2.56	1.39	
11		3	9.60	2.77	1.21			2.54	1.44	
12		4	9.20	2.72	1.21			2.57	1.35	
13		5	9.34	2.81	1.15			2.37	1.61	
14		6	9.22	2.71	1.22			2.36	1.61	
15		7	9.86	2.57	1.45	1.26	15.3/14.0	2.32	1.78	1.50
16										
17	27	1	6.07	.70	12.02			.49	24.5	
18		2	5.86	.55	18.80			.48	24.7	
19		3	5.98	.62	15.09			.49	24.2	
20		4	5.87	.62	14.82			.48	24.7	
21		5	5.95	.68	12.49			.48	25.1	
22		6	5.94	.54	19.77			.48	25.0	
23		7	5.95	.65	13.66	15.23	1.23/1.06	.48	25.0	24.7
24										
25	37	1	12.06	1.40	5.97			1.67	4.20	
26		2	11.40	1.51	4.85			1.51	4.85	
27		3	11.88	1.47	5.33	5.38	4.69/5.01	1.53	4.92	4.66
28										
29	39	1	3.66	.65	8.41			.70	7.25	
30		2	3.79	.75	6.54			.68	7.95	
		3	3.74	.68	7.85	7.60	2.82/2.60	.68	7.85	7.68

JDR 1/2/85

NCEL 12" Vertical Smooth Cylinder

	Run #[1]	Wave #[2]	F_m[3]	U_m[4]	C_m[5]	C_m[6]	K_m/K_v[7]	U_{vm}[8]	C_m[9]	Average C_m
1	40	1	7.94	1.85	2.25			1.68	2.73	
2		2	7.92	1.74	2.54			1.68	2.72	
3		3	7.80	1.69	2.65	2.48	6.88/6.39	1.67	2.71	2.72
4										
5	42	1	2.68	.79	4.17			.58	7.73	
6		2	2.77	.70	5.49			.56	8.57	
7		3	2.88	.74	5.10	4.92	3.63/2.69	.57	8.60	8.30
8										
9	43	1	8.40	2.27	1.58			2.21	1.67	
10		2	8.14	2.22	1.60			2.31	1.48	
11		3	8.62	2.30	1.58	1.59	10.7/10.8	2.34	1.53	1.56
12										
13	44	1	13.68	3.26	1.25			3.21	1.29	
14		2	14.51	3.33	1.27			3.34	1.26	
15		3	14.04	3.16	1.36	1.29	15.3/15.4	3.29	1.26	1.27
16										
17	45	1	20.15	2.25	3.86	3.86	8.53/9.64	2.29	3.73	3.73
18	Not plotted since only one wave is available									

JDR 1/2/84

61

NCEL 12" Vertical Smooth Cylinder

Run #	Wave #	T²(sec)	H³(ft)	Measured Kinematics					Stream Function Kinematics				
				C_d 4	C_m 5	RMS/Force	$R \times 10^{-5}$	K 8	C_d 9	C_m 10	RMS/Force	$R \times 10^{-5}$	K
27	1	2.00	1.05	.60	2.38	.0939	.54	1.34	1.35	2.09	.0246	.43	1.08
	2	"	1.03	.39	2.34	.0784	.53	1.32	1.71	2.09	.0214	.42	1.06
	3	"	1.04	.48	2.35	.0857	.45	1.12	.40	2.09	.0186	.43	1.07
	4	"	1.03	-.54	2.33	.0792	.46	1.16	1.54	2.08	.0211	.42	1.06
	5	"	1.02	-.84	2.34	.0787	.47	1.18	.70	2.11	.0169	.42	1.06
	6	"	1.02	-.43	2.34	.0854	.51	1.28	1.13	2.11	.0204	.42	1.05
	7	"	1.01	-.81	2.34	.0823	.49	1.23	.98	2.13	.0198	.42	1.04
Average													
37	1	3.00	2.59	-.08	2.42	.0572	1.38	5.17	-.40	1.99	.0640	1.40	5.25
	2	"	2.37	-.17	2.19	.0613	1.20	4.49	.78	1.94	.0398	1.30	4.88
	3	"	2.40	.01	2.22	.0632	1.18	4.41	.60	1.97	.0319	1.31	4.91
Average													
39	1	4.00	.93	.03	2.15	.0390	.56	2.78	-.51	1.99	.0436	.53	2.66
	2	"	.90	.03	2.14	.0627	.56	2.82	.08	2.05	.0456	.51	2.57
	3	"	.90	.07	2.14	.0583	.57	2.85	-.58	2.05	.0482	.51	2.57
Average													
40	1	4.00	2.28	.22	2.06	.0656	1.39	6.96	-.28	1.97	.0932	1.28	6.41
	2	"	2.28	.24	2.07	.0684	1.44	7.19	-.42	1.98	.0944	1.28	6.40
	3	"	2.26	.18	2.09	.0572	1.30	6.50	-.65	1.98	.0974	1.28	6.37
Average													
42	1	5.00	.74	.46	2.22	.0391	.59	3.70	-1.05	2.06	.0406	.44	2.75
	2	"	.72	.62	2.27	.0588	.60	3.72	.27	2.18	.0501	.42	2.64
	3	"	.72	.20	2.31	.0526	.56	3.47	.15	2.21	.0539	.43	2.67
Average													

JDR 1/4/85

NCEL 12" Vertical Smooth Cylinder

Run #	Wave # [1]	T (sec) [2]	H (ft) [3]	Measured Kinematics					C_d [9]	C_m [10]	Stream Function Kinematics		
				C_d [4]	C_m [5]	RMS/ϕ_{max}	$Re \times 10^{-5}$	K [8]			RMS/F_{max}	$Re \times 10^{-5}$	K
43	1	5.00	2.72	.31	1.93	.0712	1.68	10.51	.13	1.79	.0543	1.67	10.42
	2	"	2.83	.33	1.91	.0972	1.71	10.69	.04	1.71	.0725	1.74	10.87
	3	"	2.86	.34	2.00	.1028	1.73	10.83	-.09	1.80	.0712	1.76	11.00
Average													
44	1	5.00	4.24	.51	1.82	.0968	2.34	14.59	.34	1.59	.1023	2.42	15.12
	2	"	4.39	.39	1.84	.1055	2.51	15.68	.30	1.55	.1156	2.52	15.71
	3	"	4.34	.32	1.82	.1067	2.51	15.68	.29	1.55	.1307	2.48	15.49
Average													

JDR 1/4/55

Vertical Smooth 8" Cyl "δ2"

$$C_\mu = \frac{F_\mu}{U_{\mu y}\,\frac{1}{2}\,D L}\;;\; \text{where } U_{\mu y} \text{ – is from Stream function as } \cdots - \overline{\overline{x}} y$$

	Run[1] #	Wave[2] #	F_μ[3]	U_{xy}[4]	C_μ[5]	$\overline{C_\mu}$[6]	$\overline{K_\psi}$[7]	8	9	10
1	1	1	5.99	.70	8.77					
2		2	6.08	.71	8.65					
3		3	6.01	.71	8.55	8.66	2.45			
4										
5	2	1	9.73	1.18	5.01					
6		2	9.62	1.17	5.04					
7		3	9.53	1.18	4.91	4.99	4.09			
8										
9	3	1	13.92	1.84	2.95					
10		2	13.96	1.79	3.12					
11		3	14.18	1.78	3.21	3.09	6.27			
12										
13	4	1	17.46	2.35	2.27					
14		2	17.20	2.35	2.23					
15		3	17.42	2.40	2.17	2.22	8.23			
16										
17	5	1	17.71	2.46	2.10					
18		2	17.90	2.43	2.17					
19		3	17.93	2.46	2.12	2.13	8.51			
20										
21	6	1	3.94	.74	5.16					
22		2	3.79	.73	5.10					
23		3	3.83	.72	5.30	5.19	3.77			
24										
25	7	1	8.09	1.58	2.32					
26		2	8.20	1.61	2.27					
27		3	8.40	1.59	2.38	2.33	8.19			
28										
29	8	1	12.53	2.30	1.70					
30		2	12.80	2.28	1.77					
		3	12.50	2.34	1.64	1.70	11.9			

JDR 1/3/85

Vertical 8" Smooth Cyl. "82"

	Run[1] #	Wave[2] #	F_μ [3]	$U_{\mu\nu}$ [4]	C_μ [5]	$\overline{C_\mu}$ [6]	$\overline{K_\psi}$ [7]	8	9	10
1	9	1	14.61	3.12	1.08					
2		2	14.68	3.16	1.05					
3		3	13.94	3.17	.99	1.04	16.2			
4										
5	10	1	16.92	3.53	.97					
6		2	17.12	3.51	1.00					
7		3	15.83	3.51	.92	.96	18.1			
8										
9	11	1	3.01	.69	4.53					
10		2	3.33	.68	5.16					
11		3	3.56	.67	5.69	5.13	4.35			
12										
13	12	1	6.07	1.42	2.16					
14		2	6.34	1.40	2.32					
15		3	6.86	1.36	2.66	2.38	8.92			
16										
17	13	1	11.86	2.85	1.05					
18		2	11.30	2.99	.91					
19		3	11.35	3.02	.89	.95	18.9			
20										
21	14	1	14.24	3.53	.82					
22		2	14.84	3.41	.92					
23		3	15.21	3.41	.94	.89	22.1			
24										
25	15	1	2.90	.66	4.77					
26		2	2.94	.66	4.84					
27		3	3.06	.62	5.71	5.11	4.75			
28										
29	16	1	5.05	1.26	2.28					
30		2	5.12	1.30	2.17					
		3	5.42	1.23	2.57	2.34	9.29			

National , 45-385

JDR 1/3/85

Run[1] #	Wave[2] #	F_M [3]	U_{MV} [4]	C_M [5]	$\overline{C_M}$ [6]	$\overline{K_V}$ [7]	8	9	10
17	1	10.62	2.34	1.39					
	2	10.37	2.28	1.43					
	3	9.52	2.17	1.45	1.42	16.6			
18	1	13.02	3.07	.99					
	2	13.38	2.97	1.09					
	3	13.43	2.79	1.24	1.11	21.7			
19	1	4.29	1.05	2.79					
	2	4.13	1.07	2.59					
	3	4.04	1.18	2.08	2.49	9.17			
20	1	6.42	1.81	1.41					
	2	6.41	1.84	1.36					
	3	6.97	1.93	1.34	1.37	15.5			
21	1	9.71	2.38	1.23					
	2	9.52	2.27	1.32					
	3	8.92	2.39	1.12	1.22	19.6			
22	1	10.73	2.61	1.13					
	2	11.47	2.71	1.12					
	3	11.08	2.80	1.01	1.09	22.6			
23	1	5.26	.71	7.48					
	2	5.07	.70	7.42					
	3	5.34	.71	7.60	7.50	2.84			
24	1	9.69	1.41	3.50					
	2	9.42	1.44	3.26					
	3	9.46	1.42	3.36	3.37	5.75			

JDR 1/3/85

45-385 ᶜ

	Run [1] #	Wave [2] #	F_μ [3]	$U_{\mu\psi}$ [4]	C_μ [5]	$\overline{C}_\mu$ [6]	$\overline{K}_\psi$ [7]	8	9	10
1	25	1	13.03	2.05	2.22					
2		2	13.17	2.06	2.23					
3		3 -	13.26	2.07	2.22	2.22	8.31			
4										
5	26	1	18.72	2.70	1.84					
6		2	18.14	2.74	1.73					
7		3	18.60	2.67	1.87	1.82	10.9			
8										
9	27	1	19.64	3.11	1.46					
10		2	20.74	3.10	1.55					
11		3	19.59	3.09	1.47	1.49	12.5			
12										
13	32	1	18.00	2.43	2.19					
14		2	19.02	2.33	2.51					
15		3	18.82	2.36	2.42	2.37	8.26			
16										
17	33	1	15.66	3.10	1.17					
18		2	15.28	3.18	1.08					
19		3	15.05	3.13	1.10	1.12	16.2			
20										
21	34	1	9.65	1.72	2.34					
22		2	9.71	2.28	1.34					
23		3	10.67	2.18	1.61	1.76	15.2			
24										
25	35	1	9.81	2.43	1.19					
26		2	9.85	2.52	1.11					
27		3	10.03	2.67	1.01	1.10	21.2			
28										
29										
30										

JDR 1/3/85

Vertical 8" Smooth Cylinder

$$C_\mu = \frac{F_\mu}{D_\mu^2 \frac{1}{2} DL} \qquad \hat{\phi} = \frac{\theta_f - \theta_q}{\theta_c' - \theta_q} u$$

	Run # [1]	$\overline{T(sec)}$ [2]	$\overline{H(ft)}$ [3]	$\overline{K}$ [4]	$\overline{Re \times 10^{-5}}$ [5]	$\overline{\hat{\phi}}$ Peak [6]	$\overline{\hat{\phi}}$ Trough [7]	$\hat{C}_\mu$ Trough [8]	9	10
1	1	2.50	1.12	2.4	.36	0.99	1.09			
2	2	"	1.87	4.1	.60	.93	1.16			
3	3	"	2.89	6.3	.92	.90	.92			
4	4	"	3.88	8.2	1.2	.81	1.02			
5	5	"	4.05	8.5	1.2	.80	.88			
6	6	3.70	2.90	3.8	.37	.92	1.01			
7	7	"	2.08	8.2	.81	.90	.97			
8	8	"	3.00	11.9	1.2	.86	.90			
9	9	"	4.12	16.2	1.6	.63	.69			
10	10	"	4.63	18.1	1.8	.70	.76			
11	11	4.60	0.85	4.3	.35	1.00	1.00			
12	12	"	1.70	8.9	.71	.79	.83			
13	13	"	3.53	18.9	1.5	.80	.79			
14	14	"	4.11	22.1	1.8	.82	.85			
15	15	5.29	0.78	4.8	.33	.93	1.00			
16	16	"	1.49	9.3	.64	.94	.87			
17	17	"	2.59	16.6	1.2	1.06	.89			
18	18	"	3.33	21.7	1.5	.96	.84			
19	19	6.00	1.26	9.2	.56	.96	1.01			
20	20	"	2.07	15.5	.95	.92	.91			
21	21	"	2.57	19.6	1.2	.85	.94			
22	22	"	2.94	22.6	1.4	1.05	.92			
23	23	2.90	1.02	2.8	.36	.94	1.17			
24	24	"	2.07	5.7	.73	.87	1.07			
25	25	"	3.00	8.3	1.1	.81	.90			
26	26	"	4.00	10.9	1.4	.69	.81			
27	27	"	4.68	12.5	1.6	.83	.75			
28	32	2.50	3.90	8.3	1.2	.81	1.04			
29	33	3.70	4.11	16.2	1.6	.84	.87			
30	34	5.29	2.55	16.4	1.1	.77	.82			
	35	6.00	2.77	21.2	1.3	.74	.58			

JDR 12/6/84

J.R.

Smooth horizontal Oscillating Cylinder 4/20/76

D = 12 ¾"   ν assumed = 1.41×10^{-5}

$$C_M = \frac{F_M}{\frac{1}{2}\rho D U_M^2 L}$$

$$K = \frac{U_M T}{D}$$

$$Re = \frac{U_M D}{\nu}$$

Run #	Wave #	F_M (lb)	$\overline{F}_M$	U_M (ft/s)	$\phi_1 (\tfrac{1}{50}")$	$\phi_2 (\tfrac{1}{50}")$	ϕ_{AV}	$\hat{\phi}$	Average
1	2	3	4	5	6	7	8	9	10
158	1	8.87		2.36	25	23	24	.60	$C_M = .68$
T=7.85s	2	9.39		"	25	23	24	.60	$\hat{\phi} = .63$
	3	10.96		"	29	27	28	.70	$K = 17.4$
	4	10.96	10.05	"	29	22	25.5	.64	$Re = 1.77(10)^5$
									$\beta = 10,170$
159	1	77.59		4.45	26	22	24	.60	$C_M = 1.46$
T=3.92	2	77.59		"	28	20	24	.60	$\hat{\phi} = .58$
	3	75.52		"	26	19	22.5	.57	$K = 16.4$
	4	76.55	76.81	"	27	17	22	.55	$Re = 3.35(10)^5$
									$\beta = 29,430$
160	1	131.38		6.80	17	15	16	.61	$C_M = 1.08$
T=2.62	2	128.28		"	19	19	19	.71	$\hat{\phi} = .66$
	3	133.45		"	14	17	15.5	.59	$K = 16.8$
	4	132.42		"	17	21	19	.71	$Re = 5.13(10)^5$
	5	133.52		"	19	16	17.5	.66	$\beta = 30,540$
	6	136.55	132.93	"	18	20	19	.70	
161	1	345.52		7.78	14	20	17	.69	$C_M = 2.23$
T=1.96	2	357.93		"	15	22	18.5	.74	$\hat{\phi} = .72$
	3	372.41		"	15	22	18.5	.75	$K = 14.4$
	4	376.55		"	13	22	17.5	.71	$Re = 5.68(10)^5$
	5	372.41		"	15	21	18	.72	$\beta = 40,330$
	6	353.79	363.10	"	14	21	17.5	.70	
162	1	10.30		1.75	24	20	22	.55	$C_M = 1.20$
T=15.70	2	10.30		"	30	28	29	.73	$\hat{\phi} = .63$
	3	8.75	9.79	"	27	22	24.5	.62	$K = 25.9$
									$Re = 1.32(10)^5$

U_M determined from displacement measurement (u is max. where displ. is zero.) $\beta = 5,100$

ϕ_a taken when displacement is maximum.

5/28/84 JDR

Smooth Oscillating Cylinder   Test Date 4/20/76 $D = 12\tfrac{3}{4}''$

Run #	Wave #	F_M (lb)	$\overline{F_M}$	U_M (ft/s)	ϕ_1 (1/50")	ϕ_2 (1/50")	ϕ_{AV}	$\hat{\phi}$	
163	1	30.00		4.04	23	24	23.5	.59	$C_M = .63$
T=7.87	2	24.41		"	21	25	23	.58	$\hat{\phi} = .56$
	3	27.45		"	22	23	22.5	.56	$K = 29.9$
	4	28.50	27.59	"	21	19	20	.50	$Re = 3.04 \times 10^5$
									$\beta = 39,110$
164	1	75.52		6.29	27	31	29	.54	$C_M = .69$
T=5.24	2	72.41			26	33	29.5	.55	$\hat{\phi} = .58$
	3	71.38	73.10		31	37	34	.64	$K = 31.0$
									$Re = 4.74 \times 10^5$
165	1	134.69		7.23	23	18	20.5	.52	$C_M = .61$
T=3.92	2	132.65		"	27	25	26	.65	$\hat{\phi} = .58$
	3	131.63			26	20	23	.58	$K = 28.9$
	4	132.65	132.91	"	28	17	22.5	.57	$Re = 5.90 \times 10^5$
166	1	244.07		9.87	25	17	21	.53	$C_M = .54$
T=3.14	2	231.86		"	24	20	22	.55	$\hat{\phi} = .54$
	3	252.20		"	20	22	21	.53	$K = 29.2$
	4	248.14	244.06	"	22	21	21.5	.54	$Re = 7.45 \times 10^5$
									$\beta = 25,56$
167	1	7.21		1.96	20	15	17.5	.58	$C_M = .21$
T=23.58	2	6.70		"	25	17	21	.69	$\hat{\phi} = .62$
	3	5.15	6.35	"	17	18	17.5	.58	$K = 43.9$
									$Re = 1.49 \times 10^5$
168	1	23.28		4.05	14	19	16.5	.55	$C_M = .48$
T=11.78	2	20.69		"	18	15	16.5	.55	$\hat{\phi} = .58$
	3	19.14	21.04	"	20	18	19	.63	$K = 44.9$
									$Re = 3.05 \times 10^5$
169	1	50.47		5.88	20	18	19	.48	$C_M = .53$
T=7.87	2	48.41		"	23	21	22	.55	$\hat{\phi} = .54$
	3	49.96		"	22	18	20	.50	$K = 43.6$
	4	45.32	48.54	"	27	22	24.5	.61	$Re = 4.44 \times 10^5$

8/30/84 JDR

Smooth Oscillating Cylinder Test Date 4/20/76 D = 12¾"

Run #	Wave #	F_M(lb)	$\overline{F}_M$	U_M(ft/s)	$\phi_1(\tfrac{1}{50}")$	$\phi_2(\tfrac{1}{50}")$	D_{av}	$\hat{\phi}$	
170	1	102.56		8.23	30	35	32.5	.55	C_M = .56
T=5.88	2	100.51		"	15	12	13.5	.46	$\hat{\phi}$ = .50
	3	99.49	100.85	"	14	16	15	.50	K = 45.5
									Re=6.20(10)⁵
									β = 18,630
171	1	201.03		10.54	7	6	6.5	.14	C_M = .68
T=4.72	2	201.03		"	7	7	7	.14	$\hat{\phi}$ = .15
	3	196.92		"	7	6	6.5	.14	K = 46.8
	4	201.03	200.00	"	8	9	8.5	.18	Re=7.94(10)⁵
									β = 16,230
172	1	319.32		12.18	10	10	10	.25	C_M = .76
T=3.92	2	301.02		"	10	12	11	.28	$\hat{\phi}$ = .27
	3	313.22		"	7	11	9	.22	K = 44.9
	4	282.71		"	16	11	13.5	.34	Re=9.17(10)⁵
	5	292.89	301.83	"	13	9	11	.28	β = 23,420
173	1	5.95		1.72	26	18	22	.55	C_M = .50
T=31.44	2	6.72		"	19	24	21.5	.53	$\hat{\phi}$ = .49
	3	6.21	6.29	"	13	18	15.5	.39	K = 50.9
									Re=1.30(10)⁵
174	1	20.17		3.62	9	8	8	.45	C_M = .50
T=15.70	2	19.14		"	8	10	9	.44	$\hat{\phi}$ = .46
	3	18.62	19.31	"	9	11	10	.50	K = 56.4
									Re=2.88(10)⁵
175	1	40.51		6.42	30	28	29	.54	C_M = .58
T=10.47	2	39.49		"	20	21	20.5	.38	$\hat{\phi}$ = .46
	3	44.10	41.37	"	24	24	24	.45	K = 63.3
									Re=4.84(10)⁵
176	1	81.03		8.22	18	15	16.5	.41	C_M = .48
T=7.87	2	85.13		"	17	11	14	.35	$\hat{\phi}$ = .34
	3	90.26	85.47	"	11	11	11	.27	K = 60.9
									Re=6.20(10)⁵

8/30/84 JDR

Smooth Oscillating Cylinder Test Date 4/20/76 D = 12¾"

Run #	Wave #	F_m (lb)	$\overline{F}_m$	U_m (ft/s)	$\phi_1 (\tfrac{t_o}{50}")$	$\phi_2 (\tfrac{t_o}{50}")$	ϕ_{AV}	$\hat{\phi}$	average
	2	3	4	5	6	7	8	9	10
177	1	169.23		9.56	20	20	20	.32	$C_M = .70$
T = 6.29	2	:72 3		"	16	17	16.5	.26	$\hat{\phi} = .25$
	3	168.88	170.14	"	8	14	11	.17	$K = 56.6$
									$\bar{x}_e = 7.20(o)^5$
									$\beta = 15,120$
178	1	262.37		12.37	14	13	13.5	.25	$C_M = .62$
T = 5.24	2	264.41		"	11	18	14.5	.27	$\hat{\phi} = .22$
	3	242.03		"	12	8	10	.19	$K = 61.0$
	4	246.10	253.73	"	11	5	8	.15	$\bar{x}_e = 9.32(4)$
									$\beta = 15,050$
179	1	370.17		14.20	11	5	8	.17	$C_M = .70$
T = 4.48	2	384.41		"	10	9	9.5	.21	$\hat{\phi} = .18$
	3	384.41		"	7	4	5.5	.12	$K = 59.9$
	4	372.20		"	2	6	4	.09	$\bar{x}_e = 1.07(4)$
	5	368.14		"	18	4	11	.24	$\beta = 1,790$
	6	360.00	373.22	"	11	11	11	.24	

72

8/31/84 JDR

END

FILMED

9-85

DTIC